AMERICAN SOCIETY FOR MICROBIOLOGY | Journal of Virology

Impact of Heparan Sulfate Binding on Transduction of Retina by Recombinant Adeno-Associated Virus Vectors

Sanford L. Boye,[a] Antonette Bennett,[b] Miranda L. Scalabrino,[a] K. Tyler McCullough,[a] Kim Van Vliet,[b] Shreyasi Choudhury,[a] Qing Ruan,[a] James Peterson,[a] Mavis Agbandje-McKenna,[b] Shannon E. Boye[a]

Department of Ophthalmology, College of Medicine, University of Florida, Gainesville, Florida, USA[a]; Department of Biochemistry and Molecular Biology, College of Medicine, University of Florida, Gainesville, Florida, USA[b]

ABSTRACT

Adeno-associated viruses (AAVs) currently are being developed to efficiently transduce the retina following noninvasive, intravitreal (Ivt) injection. However, a major barrier encountered by intravitreally delivered AAVs is the inner limiting membrane (ILM), a basement membrane rich in heparan sulfate (HS) proteoglycan. The goal of this study was to determine the impact of HS binding on retinal transduction by Ivt-delivered AAVs. The heparin affinities of AAV2-based tyrosine-to-phenylalanine (Y-F) and threonine-to-valine (T-V) capsid mutants, designed to avoid proteasomal degradation during cellular trafficking, were established. In addition, the impact of grafting HS binding residues onto AAV1, AAV5, and AAV8(Y733F) as well as ablation of HS binding by AAV2-based vectors on retinal transduction was investigated. Finally, the potential relationship between thermal stability of AAV2-based capsids and Ivt-mediated transduction was explored. The results show that the Y-F and T-V AAV2 capsid mutants bind heparin but with slightly reduced affinity relative to that of AAV2. The grafting of HS binding increased Ivt transduction by AAV1 but not by AAV5 or AAV8(Y733F). The substitution of any canonical HS binding residues ablated Ivt-mediated transduction by AAV2-based vectors. However, these same HS variant vectors displayed efficient retinal transduction when delivered subretinally. Notably, a variant devoid of canonical HS binding residues, AAV2(4pMut)ΔHS, was remarkably efficient at transducing photoreceptors. The disparate AAV phenotypes indicate that HS binding, while critical for AAV2-based vectors, is not the sole determinant for transduction via the Ivt route. Finally, Y-F and T-V mutations alter capsid stability, with a potential relationship existing between stability and improvements in retinal transduction by Ivt injection.

IMPORTANCE

AAV has emerged as the vector of choice for gene delivery to the retina, with attention focused on developing vectors that can mediate transduction following noninvasive, intravitreal injection. HS binding has been postulated to play a role in intravitreally mediated transduction of retina. Our evaluation of the HS binding of AAV2-based variants and other AAV serotype vectors and the correlation of this property with transduction points to HS affinity as a factor controlling retinal transduction following Ivt delivery. However, HS binding is not the only requirement for improved Ivt-mediated transduction. We show that AAV2-based vectors lacking heparin binding transduce retina by subretinal injection and display a remarkable ability to transduce photoreceptors, indicating that other receptors are involved in this phenotype.

Adeno-associated viruses (AAVs) are nonpathogenic, single-stranded packaging DNA dependoparvoviruses within the family *Parvoviridae*. As the genus name implies, wild-type (WT) AAV is dependent on helper viruses, such as those in the *Adenoviridae* and *Herpesviridae* families, for replication. For its safety and the availability of a wide variety of naturally occurring serotypes displaying various tissue tropisms, recombinant AAV (rAAV) has found wide utility as both a gene therapy vector and biotechnological tool (1). Capsid crystal structures also have been determined for many of the AAV serotypes (2–9), leading to a revolution in identifying the structural determinants of receptor attachment, tropism, and transduction efficiency and, by extension, the ability to modify the capsid to generate variants with desired transduction profiles.

One of the major clinical applications of AAV is as a gene therapy vector for the treatment of blindness. The eye is a particularly well-suited organ for gene therapy due to its small size, compartmentalization, and immune-privileged status (10). Clinical trials for RPE65-Leber congenital amaurosis (LCA2) demonstrate the ability to deliver a therapeutic transgene to the retinal pigment epithelium (RPE), thereby restoring retinal function and visually evoked behavior to patients (11–13). However, the majority of inherited retinal diseases are caused by defects in photoreceptors, highlighting the need to identify serotypes capable of transducing this cell type. We and others have shown that various subretinally delivered AAV serotypes are capable of efficient transduction of photoreceptors in nonhuman primates (NHP) (14–19). However, subretinal injection of AAV2 under the fovea of some LCA2 patients led to central retinal thinning and loss of visual acuity (20). Similar decreases in retinal thickness were ob-

Received 2 February 2016 **Accepted** 4 February 2016

Accepted manuscript posted online 10 February 2016

Citation Boye SL, Bennett A, Scalabrino ML, Mccullough KT, Van Vliet K, Choudhury S, Ruan Q, Peterson J, Agbandje-Mckenna M, Boye SE. 2016. Impact of heparan sulfate binding on transduction of retina by recombinant adeno-associated virus vectors. J Virol 90:4215–4231. doi:10.1128/JVI.00200-16.

Editor: R. M. Sandri-Goldin, University of California, Irvine

Address correspondence to Mavis Agbandje-McKenna, mckenna@ufl.edu, or Shannon E. Boye, Shannon.Boye@eye.ufl.edu.

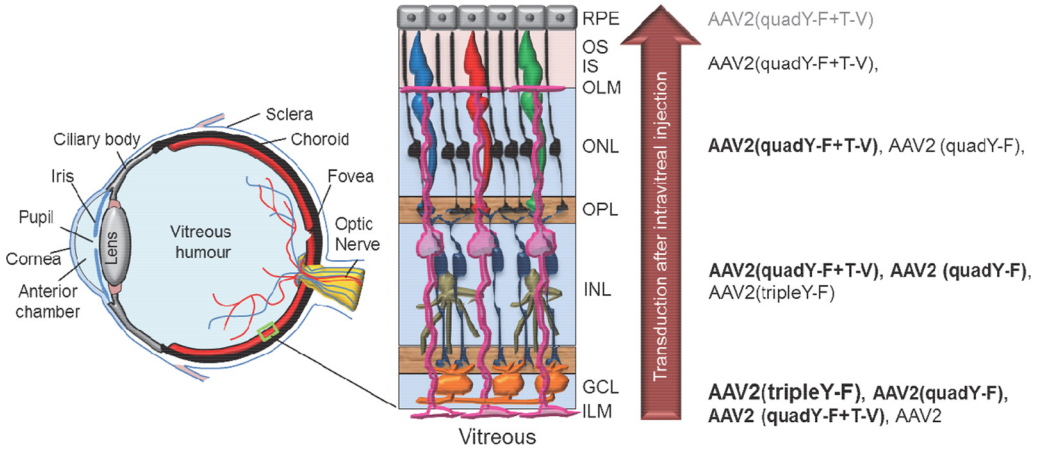

FIG 1 Schematic of the eye detailing the position of neural retina in the posterior segment, along with a higher-magnification view illustrating basic retinal anatomy. The inner limiting membrane (ILM) is a typical basement membrane at the vitreoretinal junction and is created by the end feet of Müller glia (pink). Müller glia span the entire width of the retina, forming barriers at each end, including the ILM in the inner retina and outer limiting membrane (OLM) in the outer retina. Between the ILM and OLM exist multiple nuclear and plexiform layers. The relative ability of previously described, AAV2-based vectors to transduce retinal neurons within these various layers following intravitreal injection is shown on the right. Strong transduction is depicted by large font/boldface letters, whereas weak transduction is depicted by smaller font/gray letters. While AAV2 transduces primarily ganglion cells within the inner retina, AAV2(quadY-F+T-V) promotes efficient transduction of middle retina, i.e., Müller cells (pink), bipolar cells (navy blue), horizontal cells (tan), and outer retina, i.e., photoreceptors (black/red/blue/green) and RPE (gray), following intravitreal delivery in mouse. GCL, ganglion cell layer; INL, inner nuclear layer; OPL, outer plexiform layer; ONL, outer nuclear layer; IS, inner segments of photoreceptors; OS, outer segments of photoreceptors.

served in subretinally injected NHP (21). To address the need for a safer, less invasive delivery route, attention now is focused on developing AAV vectors that can transduce outer retina (i.e., photoreceptors/RPE) following intravitreal (Ivt) injection.

There are a number of barriers to the transduction of the outer retina by Ivt-delivered AAVs, the first of which is dilution effect. The human vitreous volume is approximately 4 ml. If vitrectomy is not performed, an injection volume no greater than 100 μl is considered safe (22). This amounts to a 1:40 dilution of the delivered vector. Second, the vitreoretinal junction, composed primarily of the inner limiting membrane (ILM), a basement membrane formed by the end feet of Müller glia, poses both a physical and biological barrier (23). Lastly, there are several layers of neurons located in the inner and middle retina, anterior to the photoreceptors and RPE, which also pose a barrier. Of the naturally occurring AAV serotypes tested, only AAV2 leads to significant transduction of retina when delivered to the vitreous (23). This observation is likely because AAV2's primary cellular attachment receptor, heparan sulfate (HS), is a component of the ILM and is present in the form of heparan sulfate proteoglycan (HSPG) (24, 25). A group of basic amino acid residues responsible for HS binding (R484, R487, K532, R585, and R588) has been identified experimentally and structurally mapped to the wall of the protrusions surrounding the icosahedral 3-fold axis of symmetry of the capsid (26–29). It has been established that AAV2 accumulates at the vitreoretinal junction, presumably via its interaction with HS receptors within the ILM (23). This scenario is supported by the observation that AAV serotypes that bind sialic acid (e.g., AAV5), which is absent from the ILM, do not accumulate (23, 30). AAV5 fails to transduce healthy/intact rodent retina when delivered by Ivt injection, despite being highly efficient in RPE and photoreceptors when delivered directly to the subretinal space (31–33). Indeed, of the AAV serotypes evaluated in the eye, those that bind HS transduce retina via the vitreous, suggesting that HS binding plays a key role in the ability of vectors to mediate transduction (23, 32, 34).

The rational design of the AAV capsid to avoid proteosomal degradation enhances transduction efficiencies (30, 35–38). This is accomplished by the substitution of surface-exposed residues that otherwise would be phosphorylated and thereby target the capsid for ubiquitin-dependent proteasomal degradation. AAV2 variants containing surface-exposed tyrosine-to-phenylalanine (Y-F), threonine-to-valine (T-V), or serine-to-valine mutations or a combination of these mutations exhibit increased transduction efficiency in several tissues and organs, including the retina (30, 35, 38). Figure 1 depicts the various cell types encountered by intravitreally injected AAVs and the relative ability of the rationally designed AAV2 mutant vectors to penetrate through the retina. Initial contact occurs with the end feet of Müller glia (pink), which form the ILM. Müller glia span the entire thickness of the neural retina and form the outer limiting membrane (OLM) barrier at the opposite extreme. Next are retinal ganglion cells, followed by middle retinal cells, such as bipolars. Finally, in the outer retina are rod-and-cone photoreceptors and RPE. While AAV2(tripleY-F) very effectively transduces inner/middle retina via the vitreous, the AAV2(quadY-F) variant promotes the transduction of distal retinal neurons, including photoreceptors (38). In addition, the inclusion of a T-V mutation on top of AAV2(quadY-F) produced a variant, AAV2(quadY-F+T-V), which was capable of transducing up to 25% of photoreceptors following Ivt injection (30). Notably, when evaluated *in vitro* (ocular and nonocular cell lines) or for hepatic gene transfer, AAV2(quadY-F) has lower transduction efficiency than other variants containing fewer Y-F mutations (37, 39). The mechanism for the enhanced retinal penetration of AAV2(quadY-F) and AAV2(quadY-F+T-V) relative to that of other AAV2-based vectors has yet to be established.

The purpose of this study was to explore how HS binding mod-

TABLE 1 Summary of specific Y-F and/or T-V substitutions in the AAV2 *cap* gene

Capsid nomenclature	Mutation(s)
AAV2	None
AAV2(tripleY-F)	Y444F, Y500F, Y730F
AAV2(quadY-F)	Y272F, Y444F, Y500F, Y730F
AAV2(quadY-F+T-V)	Y272F, Y444F, Y500F, Y730F, T491V
AAV5	None

TABLE 2 Summary of HS variants engineered and tested[a]

Capsid nomenclature	Mutations
AAV2(tripleY-F+T-V) [also called AAV2(4pMut)]	Y444F, Y500F, Y730F, T491V
AAV2(4pMut)+R-S	Y444F, Y500F, Y730F, T491V, **R585S**
AAV2(4pMut)+R-T	Y444F, Y500F, Y730F, T491V, **R588T**
AAV2(4pMut)+R-S+R-T	Y444F, Y500F, Y730F, T491V, **R585S**, **R588T**
AAV2(4pMut)+R-S+R-T+R-G [also called AAV2(4pMut)ΔHS]	Y444F, Y500F, Y730F, T491V, **R585S**, **R588T**, **R487G**

[a] All variants were built from AAV2(4pMut) capsid containing three Y-F and one T-V substitution. AAV2 canonical HS binding residues were replaced with structurally equivalent residues from non-HS binder AAV5. Substitutions of canonical HS residues are in boldface.

ulates retinal transduction by AAV vectors. We first investigated heparin binding of AAV2-based Y-F and Y-F+T-V variants. Second, we explored whether HS binding enhanced retinal transduction from Ivt delivery by engrafting HS binding residues from AAV serotypes known to interact with HS onto those that do not. Using structural information, we next created a series of AAV2-based mutants with altered heparin affinities and determined their transduction profiles *in vitro* and following Ivt or subretinal injection in mice. With a subset of these vectors, we next quantified rod photoreceptor versus non-rod photoreceptor transduction following either Ivt or subretinal injection. Lastly, we evaluated the relative thermodynamic capsid stabilities of WT AAV2, a selected group of AAV2-based capsid mutants, and AAV5. Our results confirm that AAV variants best suited for retinal transduction via the vitreous are those that bind HS, including those that display penetrating ability. Those variants with enhanced photoreceptor transduction from the vitreous have modestly reduced affinity for heparin relative to that of WT AAV2. Analyses of the AAV2 capsid structure reveals that the Y-F and T-V mutations do not interact with canonical HS binding residues on the AAV2 capsid but are proximal to this receptor interaction site. Additionally, there was a correlation between capsid stability and enhanced retinal penetration by variants. The grafting of HS binding to AAV1 by the singlet addition of the E531K mutation results in a vector phenotypically similar to AAV6, i.e., capable of significant Ivt-mediated transduction. However, while grafting of AAV2 HS residues onto other non-HS binding serotypes [AAV5 and AAV8(Y733F)] confers binding to heparin, this feature alone does not confer retinal transduction from the vitreous. We show that AAV2-based variants deficient in HS binding do not transduce retina via the vitreous. However, they efficiently transduce outer retina when delivered to the subretinal space, suggesting that another ligand and receptor are responsible for cellular entry in photoreceptors. Notably, an AAV2-based vector with multiple Y-F and T-V mutations and devoid of canonical HS binding residues, AAV2(4pMut)ΔHS, was highly efficient at transducing photoreceptors and displayed the ability to spread across the entire mouse retina. Together, these results establish that AAV-mediated retinal transduction via the vitreous is dependent on HS binding and, for subretinal vector delivery, that the ablation of HS binding of AAV2-based vectors may be an effective strategy for enhancing biodistribution to photoreceptors.

MATERIALS AND METHODS

Cell lines. HEK293 cells (originally obtained from Nicholas Muzyczka, University of Florida) and 661W cells (originally obtained from Muayyad R. Al-Ubaidi, University of Oklahoma) were passaged by dissociation in 0.05% (wt/vol) trypsin and 0.02% (wt/vol) EDTA, followed by replating at split ratios from 1:3 to 1:6 in T75 flasks. Experiments were conducted on cells between passages 37 and 50 for HEK293 cells and 28 to 30 for 661W cells. Cell morphology and growth rates were closely monitored to ensure cell line identity throughout passages. Cells were maintained in Dulbecco's modified Eagle's medium (DMEM) containing 5% fetal bovine serum (FBS) and 50 mg/ml Gentamicin and incubated at 37°C in 7% CO_2.

Animals. rAAV-mCherry vectors were injected into 1-month-old C57Bl/6J mice or *Nrl*-green fluorescent protein (GFP) mice, and rAAV-Luc vectors were injected into 6-week-old BALB/c mice. All mice originated from Jackson Laboratories (Bar Harbor, ME), were maintained in the University of Florida Health Science Center's animal care facilities, and were handled in accordance with the ARVO statement for the use of animals in ophthalmic and vision research and the guidelines of the Institutional Animal Care and Use Committee of the University of Florida. Animal work performed in this study was approved by UF's IACUC (animal protocols 201207573 and 201408321).

Recombinant WT and mutant AAV vector production and purification. Recombinant AAV1-, AAV2-, AAV5-, and AAV8-based capsid mutants were generated by site-directed mutagenesis of the appropriate *rep-cap* plasmids, pACG2R1C (AAV1), pACG-2 (AAV2) (40), pACG2R5C (AAV5) (40), and p5E18-VD2/8 (AAV8) (41), using the QuikChange multi-site-directed mutagenesis kit (200514; Agilent Technologies, CA) or by standard molecular cloning of synthetic DNA elements containing the mutated sequence into the appropriate *rep-cap* plasmids. For most of the vectors, site-directed mutagenesis or cloning of synthetic fragments of *cap* also introduced silent changes that added or removed restriction endonuclease sites, thereby aiding in screening. Mutated or altered *cap* genes were fully sequenced prior to vector packaging. Existing AAV2 Y-F and Y-F+T-V capsid variants have been described in prior publications (30, 37). Specific residues mutated in the AAV2 *cap* gene and their combinations are presented in Tables 1 and 2. A full summary of all mutants used in animal studies and their respective titers are presented in Table 3. Self-complementary rAAV vector constructs containing the small chimeric cytomegalovirus (CMV)/chicken beta-actin promoter (smCBA) driving mCherry or standard rAAV constructs containing the photoreceptor-specific human rhodopsin kinase-1 (hGRK1) driving mCherry were packaged in all or a select group of capsid variants for use in ocular injections. For intravascular delivery, an rAAV vector construct containing the smCBA promoter driving the firefly luciferase (Luc) cDNA was packaged in a select number of variants.

The detailed methodology of vector production and purification has been described previously (40). Briefly, vectors were packaged using a plasmid-based system in HEK293 cells by $CaPO_4$ double or triple transfection. Cells were harvested and lysed by successive freeze-thaw cycles. Virus within the lysate was purified by discontinuous iodixanol step gradients, followed by further purification via column chromatography on a 5-ml HiTrap Q Sepharose column using a Pharmacia AKTA fast pressure liquid chromatography (FPLC) system (Amersham Biosciences, Piscataway, NJ, USA). Vectors then were concentrated and buffer exchanged

TABLE 3 Summary of rAAV vectors used in *in vivo* animal experiments

Capsid name and assessment type[a]	Construct	Amt delivered (vg)	Mutation(s)
Qualitative assessment of transduction following Ivt and subret delivery			
AAV1	Sc-smCBA-mCherry	1×10^{10}	
AAV1(E531K)	Sc-smCBA-mCherry	2×10^{10}	E531K
AAV6	Sc-smCBA-mCherry	2×10^{10}	None
AAV5	Sc-smCBA-mCherry	2×10^{9}	None
AAV5+HS	Sc-smCBA-mCherry	2×10^{9}	S575R, S576G, T577N, T578R
AAV8(Y733F)	Sc-smCBA-mCherry	2×10^{9}	Y733F
AAV8(Y733F)+HS	Sc-smCBA-mCherry	6×10^{9}	Y733F, Q588R, Q589G, T591R
AAV2	Sc-smCBA-mCherry	2×10^{9}	None
AAV2(quadY-F+T-V)	Sc-smCBA-mCherry	1×10^{10}	Y272F, Y444F, Y500F, Y730F, T491V
AAV2(tripleY-F+T-V), i.e., AAV2(4pMut)	Sc-smCBA-mCherry	1×10^{10}	Y444F, Y500F, Y730F, T491V
AAV2(4pMut)+R-S	Sc-smCBA-mCherry	2×10^{10}	Y444F, Y500F, Y730F, T491V, R585S
AAV2(4pMut)+R-T	Sc-smCBA-mCherry	2×10^{9}	Y444F, Y500F, Y730F, T491V, R588T
AAV2(4pMut)+R-S+R-T	Sc-smCBA-mCherry	4×10^{10}	Y444F, Y500F, Y730F, T491V, R585S, R588T
AAV2(4pMut)ΔHS	Sc-smCBA-mCherry	1×10^{10}	Y444F, Y500F, Y730F, T491V, R585S, R588T, R487G
AAV2	Sc-smCBA-mCherry	5×10^{9}	None
AAV2(quadY-F+T-V)	Sc-smCBA-mCherry	5×10^{9}	Y272F, Y444F, Y500F, Y730F, T491V
AAV2(4pMut)	Sc-smCBA-mCherry	5×10^{9}	Y444F, Y500F, Y730F, T491V
AAV2(4pMut)ΔHS	Sc-smCBA-mCherry	5×10^{9}	Y444F, Y500F, Y730F, T491V, R585S, R588T, R487G
AAV5	Sc-smCBA-mCherry	5×10^{9}	None
Quantitative assessment of photoreceptor-specific transduction following Ivt and subret delivery			
AAV2(quadY-F+T-V)	GRK1-mCherry	Multiple[b]	Y272F, Y444F, Y500F, Y730F, T491V
AAV2(4pMut)	GRK1-mCherry	Multiple[b]	Y444F, Y500F, Y730F, T491V
Quantitative assessment of liver transduction following intravascular delivery			
AAV2	smCBA-LUC	2×10^{11}	None
AAV2(4pMut)MAX ΔHS	smCBA-LUC	2×10^{11}	Y444F, Y500F, Y730F, T491V, R585S, R588T, R487G
AAV2(quadYF+T-V)	smCBA-LUC	2×10^{11}	Y272F, Y444F, Y500F, Y730F, T491V

[a] Subret, subretinal.
[b] For Ivt injection, 4×10^{9} and 4×10^{10}; for subret injection, 2×10^{9} and 1×10^{10}.

into Alcon BSS (sodium, 155.7 mM; potassium, 10.1 mM; calcium, 3.3 mM; magnesium, 1.5 mM; chloride, 128.9 mM; citrate, 5.8 mM; acetate, 28.6 mM; osmolality, 298 mOsm) supplemented with Tween 20 (0.014%). Virus titers were determined by quantitative PCR (qPCR) relative to a standard and stored at −80°C as previously described (21).

Heparin columns. WT and variant rAAV vectors, at 200 to 400 ng in PBS-MK buffer (1× phosphate-buffered saline [PBS], 1 mM $MgCl_2$, 2.5 mM KCl), were loaded onto an equilibrated 300-μl heparin column (H6508; Sigma), and the flowthrough was collected by gravity flow. The column was washed with 5 column volumes of PBS-MK buffer, and bound virus was eluted with increasing concentrations of NaCl in PBS-MK buffer in 50 mM increments. The load, wash, and elution fractions were boiled at 100°C for 10 min and analyzed by dot blotting. The samples were loaded on a nitrocellulose membrane and immunoblotted with primary antibody B1 (American Research Products, Inc., Waltham, MA), which recognizes a linear epitope at the C terminus of the AAV viral proteins and a horseradish peroxidase (HRP)-linked anti-mouse secondary antibody from sheep (GE Healthcare Life Sciences, Pittsburgh, PA). These experiments were conducted in triplicate. For AAV2-based variants, column saturation was confirmed by signal in the flowthrough for all samples. Average pixel intensity within the blot was measured in ImageJ using a template circle centered over each spot. Arbitrary values ranging from 0 (white) to 255 (black) were plotted.

Negative-stain electron microscopy of capsids. Five microliters of the rAAV vectors was loaded onto a carbon-coated copper electron microscope (EM) grid (Ted Pella, Inc., Redding, CA), incubated for 2 min, and negatively stained with 2% uranyl acetate. The EM grids were examined with an FEI Spirit Transmission EM operated at 120 kV, and the images were collected at ×46,000 magnification with a Gatan 2,000- by 2,000-pixel charge-coupled device (CCD) camera.

Differential scanning fluorescence (DSF) stability assay. Approximately 23-μl aliquots of rAAV vectors at ~0.1 mg/ml were incubated with 2.5 μl of 1% Sypro-orange (Bio-Rad Laboratories, Inc., Hercules, CA.) in 96-well format PCR plates for analysis in a myIQ PCR instrument (Bio-Rad). The temperature was gradually increased from 30°C to 99°C at a rate of 0.5°C every 10 s, and the rate of change of fluorescence was measured. The melting temperature (T_m) was determined to be the maximum value of the first derivative of the rate of change of fluorescence with temperature. This point represents a stage at which 50% of the sample has denatured.

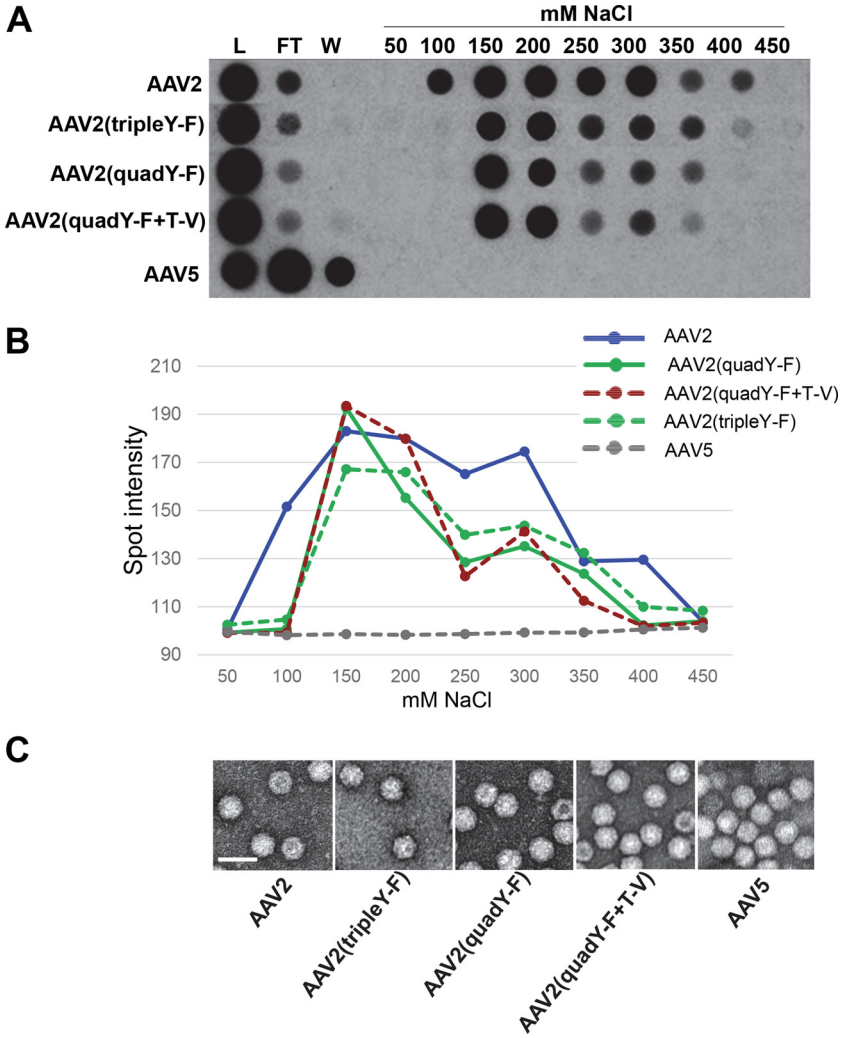

FIG 2 Heparin binding assay and electron micrographs of various AAV2-based recombinant vectors containing tyrosine-to-phenylalanine and/or threonine-to-valine substitutions. (A) The heparin binding elution profiles of AAV2 (positive control), AAV2 mutants (tripleY-F, quadY-F, and quadY-F+T-V), and AAV5 (negative control) at different salt concentrations. (B) Quantification of HS binding data from panel A. (C) Negative-stain electron micrographs of the corresponding vectors from panel A observed at ×46,000 magnification. White scale bars are 50 nm in length and are located at the bottom left of each micrograph. L, load; FT, flowthrough; W, wash.

Visualization of surface mutations on AAV capsid. To visualize the location of the residue mutations on the AAV capsid surfaces, the VP3 monomer coordinates for AAV2 (1LP3), AAV5 (3NTT), and AAV8 (2QA0) were downloaded from the RCSB website (www.rcsb.org). The appropriate residues were interactively mutated in the VP3 coordinates using the COOT program (42). The mutated monomer coordinates were used to generate capsid surface icosahedral asymmetric unit "roadmaps" from a monomer in a standard icosahedral orientation using the RIVEM program (43). The mutated VP3 monomers also were used to generate 60mer coordinates by icosahedral matrix multiplication in the Viperdb online server (http://viperdb.scripps.edu/oligomer_multi.php). The 60mer coordinates were used to generate capsid surface images using the PyMol program (44).

Quantification of rAAV vector transduction *in vitro*. rAAV infections of HEK293 and 661W cells followed previously described methods, with minor variations (39). Cells were plated in 96-well plates at a concentration of 20,000 cells/well. The following day, they were infected with rAAV vectors at 5,000, 10,000, or 50,000 vector particles/cell. Three days postinfection, cells were dissociated with Accutase solution (MP Biomedicals, Solon, OH), and 10,000 cells per sample were counted and analyzed using a BD LSR II flow cytometer equipped with BD FACSDIVA 6.2 software (BD Biosciences, San Jose, CA). Uninfected control cells also were counted and analyzed to establish transduction efficiency baselines. Data were obtained from three samples for each vector. mCherry fluorescence was quantified with a PETexas-Red-A filter with an excitation wavelength of 532 nm and an emission band pass of 600 to 620 nm. The transduction efficiency of each AAV serotype then was calculated by multiplying the percentage of cells positive for mCherry by the mean fluorescence intensity. The values of three samples for each vector then were averaged to obtain a final transduction efficiency value for each serotype.

Ocular injections. Ivt rAAV vector injections were performed as previously described (30). Extreme care was taken to ensure that the retina was not perforated during the procedure so as to avoid leakage of vector into the subretinal space. This was confirmed visually for each injection using a Nikon SMZ800 dissecting microscope fitted with an Olympus C-4040 camera and F1.8 super bright zoom lens. If a perforation was suspected, that eye was excluded from the study. Subretinal injections were performed as previously described (45). Analysis was carried out only on animals that received comparable, successful injections (>60% retinal detachment with no surgical complications). For qualitative exper-

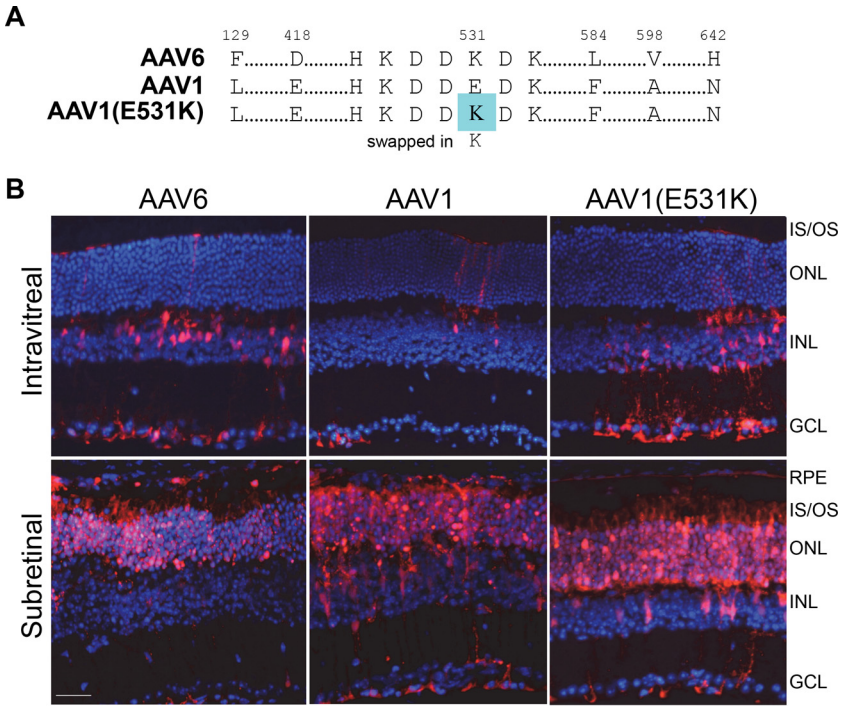

FIG 3 Capsid sequences of rAAV6, rAAV1, and rAAV1(E531K) and their transduction profiles following intravitreal or subretinal injection of rAAV in mouse retina. (A) rAAV1(E531K) is grafted with the HS binding determinant of AAV6 via a glutamic acid-to-lysine (E-K) substitution at position 531. (B) rAAV6-, rAAV1-, and rAAV1(E531K)-mediated mCherry expression (red) following Ivt or subretinal injection of between 1×10^{10} and 2×10^{10} vector genomes in C57BL/6J mice. IS/OS, inner segments/outer segments of photoreceptors; ONL, outer nuclear layer; INL, inner nuclear layer; GCL, ganglion cell layer. Scale bar, 34 μm.

iments involving rAAV6, rAAV1, and rAAV1(E531K), 1 μl of vector-containing solution was delivered subretinally or intravitreally to C57Bl/6J mice at titers ranging from 1×10^{10} to 2×10^{10} vg/μl. For qualitative experiments involving Ivt or subretinal injections of rAAV2, rAAV2(quadY-F+T-V), rAAV2(4pMut), rAAV2(4pMut)ΔHS, and all other HS capsid variants containing smCBA-mCherry, 1 μl of vector-containing solution was delivered to C57Bl/6J mice at titers ranging from 2×10^{9} to 2×10^{10} vg/μl. A total of 5 mice were used per vector and per injection route in the aforementioned experiments. For the quantification experiment evaluating Ivt or subretinal injection of rAAV2, rAAV2(quadY-F+T-V), rAAV2(4pMut), and AAV2(4pMut)ΔHS vectors, 1 μl of vector-containing solution was delivered at an identical titer (5×10^{9} vg/μl) to all Nrl-GFP mice. All cohorts contained at least three mice with the exception of mice subretinally injected with AAV5 ($n = 2$). For the quantification experiment evaluating rAAVs containing hGRK1-mCherrry, 1 μl of AAV2(4pMut)- or AAV2(quadY-F+T-V)-containing solution was delivered intravitreally at high (4×10^{10} vg/μl) or low (4×10^{9} vg/μl) doses or subretinally at high (1×10^{10} vg/μl) or low (2×10^{9} vg/μl) doses. Each cohort contained 5 mice. Concentrations for all rAAVs used in animal experiments are summarized in Table 3.

Intravascular injections of rAAV-Luc and *in vivo* bioluminescence imaging. Intravascular delivery of rAAV-Luc was achieved by direct injection of virus-containing solution into the retro-orbital venous sinus of 6-week-old BALB/c mice as previously described (46). Vector (2×10^{11} total vg) was delivered in a 100-μl volume using a 28-gauge needle. Treatment groups were $n = 3$ for AAV2, $n = 4$ for AAV2(4pMut)ΔHS, and $n = 3$ for AAV2(quadY-F+T-V). Four weeks following rAAV-Luc injection, mice were anesthetized with 2% isoflurane, administered luciferin substrate (Life Technologies, Grand Island, NY), and imaged 3 min later for bioluminescence using the Xenogen IVIS Lumina system (Caliper Life Sciences, Hopkington, MA). The analysis of relative signal intensity was done using Living Image 3.2 software (Caliper Life Sciences, Hopkington, MA).

Quantification of rAAV vector transduction *in vivo*. Four weeks after subretinal or intravitreal injection with rAAV2, rAAV2(4pMut)ΔHS, rAAV2(4pMut), rAAV2(quadY-F+T-V), or rAAV5 vectors containing smCBA-mCherry in Nrl-GFP mice, mCherry expression was documented using a Micron III fundoscope (Phoenix Research Laboratories, Pleasanton, CA) with a red fluorescent filter. mCherry expression was similarly documented at 6 weeks after subretinal or intravitreal injection of AAV2(4pMut) or AAV2(quadY-F+T-V) vectors containing hGRK1-mCherrry in C57Bl/6J mice. Exposure settings were identical for imaging all intravitreally or subretinally injected mice, with intravitreally injected retinas requiring a relatively longer exposure. Immediately following fundoscopy, mice were enucleated and eyes from three Nrl-GFP or C57Bl/6J mice were fixed, dissected, sectioned, and stained as described below. In addition, neural retinas from between 3 and 6 Nrl-GFP eyes per cohort were harvested, taking care to remove retinal pigment epithelium, and dissociated with papain (3150; Worthington Biochemical Corporation, Lakewood, NJ) as previously described (30). Fluorescence-activated cell sorter (FACS; BD LSR equipped with FCS Expression, version 4, flow research edition, software; BD Biosciences, San Jose, CA) was performed on treated, dissociated retinas from Nrl-GFP mice and untreated controls to quantify the percentage of cells that were positive for GFP (i.e., rod photoreceptors), mCherry (non-rod retinal neurons or Müller glia transduced by rAAV), or both (rod photoreceptors transduced by rAAV). Non-rod transduction percentages were calculated by dividing values from the lower-right quadrant by the product of the values of the lower right plus values of the lower left times 100. Rod transduction percentages were calculated by dividing values from the upper right by the product of upper-right values plus upper-left values times 100. The percentages of rods and non-rod neural retinal cells transduced by each vector via each injection route were separately averaged. Two-tailed, unpaired *t* tests were used to statistically compare transduction efficiencies, with significance defined as a P value of <0.05. For the quantification of photoreceptor transduction by the rAAV vectors carrying the photoreceptor-specific

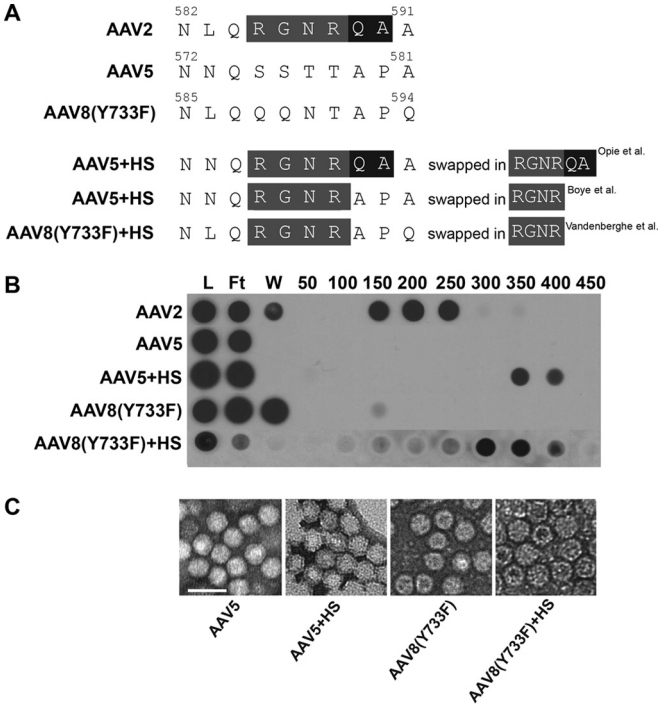

FIG 4 Capsid sequences, heparin binding, and electron micrographs of AAV5 and AAV8(Y733F) variants designed to bind HS. (A) Residues of AAV2 that were inserted into AAV5 and AAV8(Y733F) are highlighted in gray, with additional residues inserted by Opie et al. highlighted in black (29). (B) The heparin binding elution profiles of AAV2 (positive control), AAV5, and AAV8(Y733F) variants compared to those of their parent vectors AAV5 and AAV8(Y733F) (negative controls) at different salt concentrations. (C) Negative-stain electron micrographs of the corresponding vectors from panels A and B are visualized at ×46,000 magnification. Scale bar in panel C, 50 nm. L, load; FT, flowthrough; W, wash.

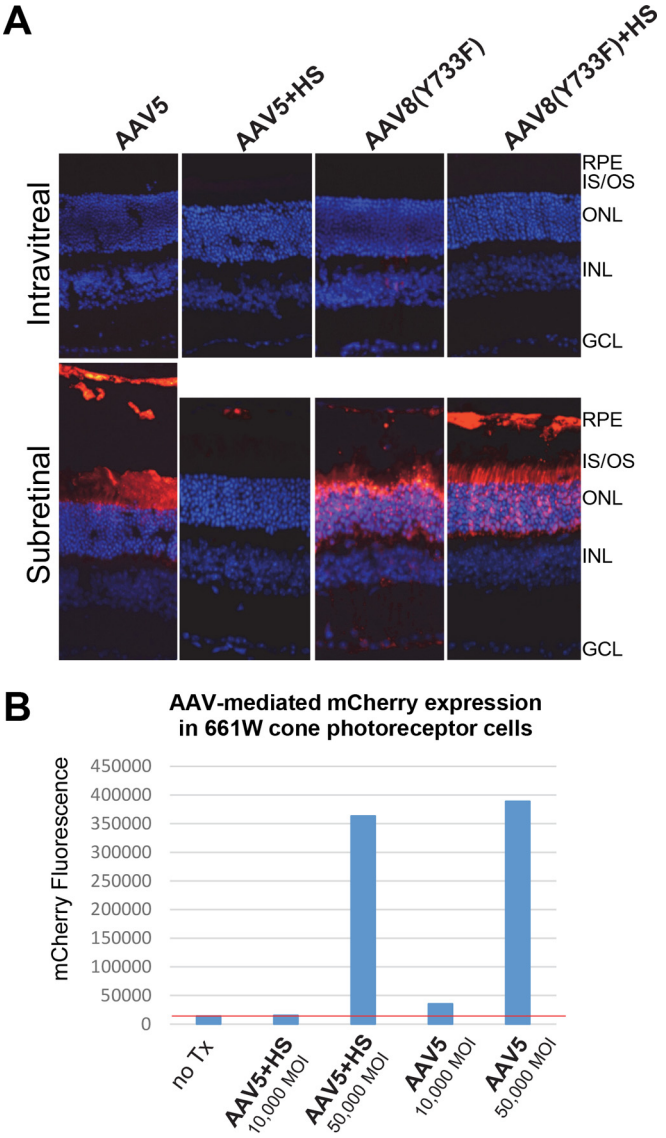

FIG 5 (A) rAAV5-, rAAV5+HS-, rAAV8(Y733F)-, and rAAV8(Y733F)+HS-mediated mCherry expression (red) following subretinal or intravitreal injection of between 2×10^9 and 6×10^9 vector genomes in C57BL/6J mice. The image of retina receiving AAV5 by subretinal injection was extended vertically to allow for visualization of transduction of RPE that was detached during the processing of tissue. IS/OS, inner segments/outer segments of photoreceptors; ONL, outer nuclear layer; INL, inner nuclear layer; GCL, ganglion cell layer. Scale bar, 34 μm. (B) Transduction efficiency of unmodified AAV5 and AAV5+HS in 661W cone photoreceptor cells. Vectors were used at multiplicities of infection (MOI) of 10,000 and 50,000. mCherry expression was calculated with FACS by multiplying the percentage of positive cells by the mean fluorescence intensity in each sample. The red line indicates the value under which all signal is noise (no transduction is observed relative to that of blank cells).

hGRK1-mCherry construct, fundus images were taken centered on the optic nerve. Images of all subretinal or Ivt-injected eyes were taken at the same exposure, excitation intensity, and gain. Pixel intensity in the red channel was quantified in each eye using ImageJ (http://imagej.nih.gov/ij/; National Institutes of Health) and averaged across the entire fundus image. These values (arbitrary units of 1 to 255) then were averaged within each cohort ($n = 3$) and compared using two-tailed unpaired t tests, with significance defined as a P value of <0.05.

Immunohistochemistry and microscopy. Eyes from Nrl-GFP and C57Bl/6J mice were enucleated (at 4 and 6 weeks postinjection, respectively) and fixed in 4% paraformaldehyde for ~12 h. Eyecups were dissected and prepared for sectioning according to previously described methods (47). Ten-micron retinal sections throughout the eyecup were cut and stored at −80°C. Retinal sections were rinsed in 1× PBS (3 times for 10 min each), incubated in Triton X-100 (30 min) and then 1% bovine serum albumin (BSA)–0.3% Triton X-100 (30 min), and rinsed again in 1× PBS (3 times for 10 min each). A subset of retinal sections from treated Nrl-GFP mice were stained with primary antibodies directed against cone arrestin (rabbit polyclonal, 1:10; generously provided by Clay Smith), purkinje cell protein 2 (PCP2) (rabbit polyclonal, 1:200; sc-68356; Santa Cruz), and calbindin (rabbit polyclonal, 1:750; AB1778; Millipore) to label cones, ON bipolar cells, and horizontal cells, respectively. Incubation in primary antibodies (4°C overnight) was followed by a 1-h incubation in Cy5-conjugated goat-anti rabbit secondary antibody (1:500; A10523; Invitrogen). All were counterstained with 4′,6′-diaminio-2-phenylindole (DAPI) for 5 min. Retinal sections (20× and 40×) were imaged using spinning-disk confocal microscopy (Nikon Eclipse TE2000 microscope equipped with the PerkinElmer Ultraview modular laser system and Hamamatsu O-RCA-R2 camera). All images were analyzed for native mCherry or Cy5-labeled cone arrestin, PCP2 or calbindin, and DAPI expression using appropriate laser lines/filter settings. All settings (exposure, gain, and laser power) were identical for each respective magnification. Entire eyecups from each mouse were visualized, and representative images from areas that fairly represented transduction within each cohort were captured. For subretinally injected eyes, images were acquired within

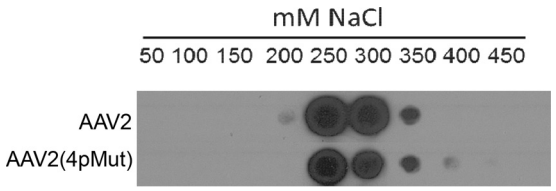

FIG 6 Heparin binding of rAAV2 and rAAV2(4pMut) capsids. Heparin binding elution profiles of AAV2(4pMut) and AAV2 (for comparison) at different salt concentrations.

the bleb. Care was taken to avoid areas of extremely high or low transduction, the optic nerve head, or extreme peripheral retina.

RESULTS AND DISCUSSION

AAV2 Y-F and Y-F+T-V variants bind HS. AAV2-based variants containing multiple Y-F and Y-F+T-V mutations were evaluated for their affinities to HS by heparin affinity column chromatography. All variants tested bound heparin, while AAV5, the negative control, did not (Fig. 2A and B). The AAV2 variants all bound HS with slightly reduced affinity relative to that of WT AAV2, including the AAV2(quadY-F) and AAV2(quadY-F+T-V) variants shown previously to be capable of photoreceptor transduction via

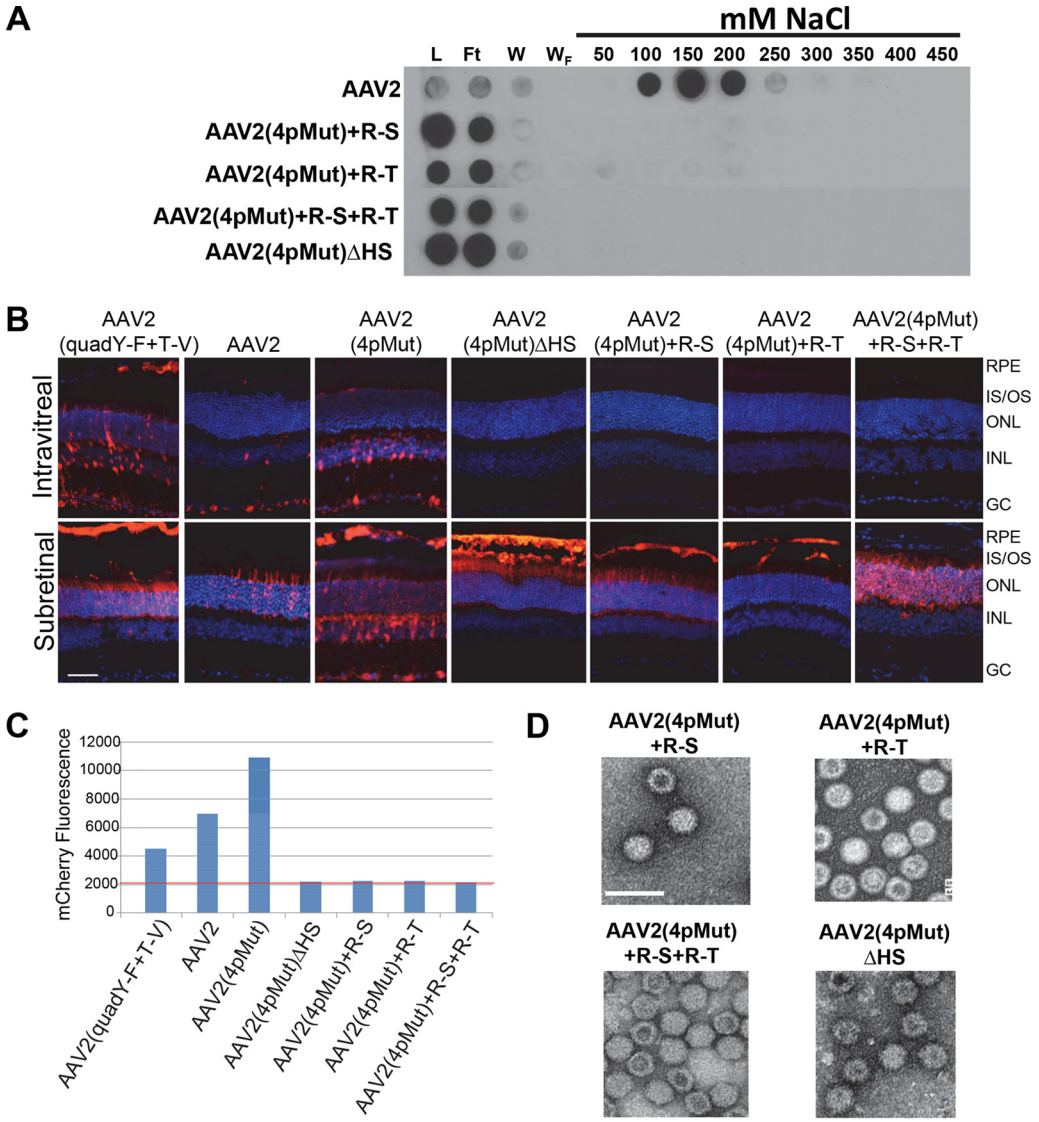

FIG 7 (A) Heparin binding elution profiles of the different AAV2 HS variants along with AAV2 (positive control) and AAV5 (negative control) at different salt concentrations. (B) mCherry expression (red) following Ivt or subretinal injection of between 2×10^9 and 4×10^{10} vector genomes in C57BL/6J mice of rAAV2(quadY-F+T-V), rAAV2, rAAV2(4pMut), rAAV2(4pMut)+R-S, rAAV2(4pMut)+R-T, rAAV2(4pMut)+R-S+R-T, and rAAV2(4pMut)+R-S+R-T+R-G [also called AAV2(4pMut)ΔHS]. (C) Transduction efficiency of AAV2 variants in HEK293 cells. All vectors were used at a multiplicity of infection (MOI) of 5,000. mCherry expression is shown in arbitrary units on the *y* axis, calculated by multiplying the percentage of positive cells by the mean fluorescence intensity in each sample. The red line indicates the value under which all signal is noise (no transduction is observed relative to that of blank cells). (D) Negative-stain electron micrographs of the corresponding vectors from panel A observed at ×46,000 magnification. L, load; FT, flowthrough; W, wash; IS/OS, inner segments/outer segments of photoreceptors; ONL, outer nuclear layer; INL, inner nuclear layer; GCL, ganglion cell layer. Scale bar in panel A, 40 μm. Scale bar in panel D, 50 nm.

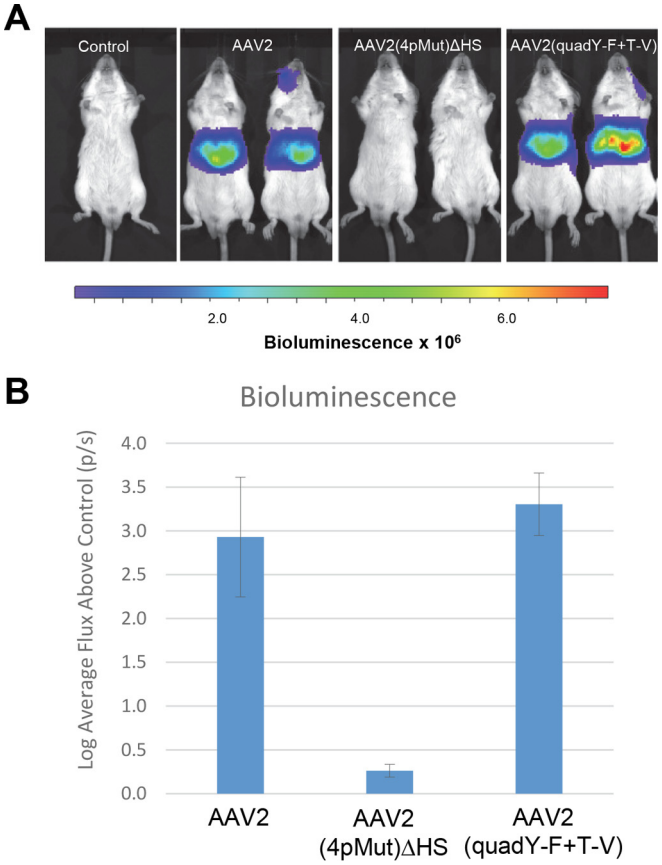

FIG 8 *In vivo* imaging of luciferase gene expression at 4 weeks postintravascular delivery of AAV2, AAV2(4pMut)ΔHS, or AAV2(quadY-F+T-V). All vectors were delivered by injection to the retro-orbital venous sinus at a dose of 2×10^{11} vector genomes. (A) Comparison of live images of bioluminescence from two representative mice (ventral position) per cohort. (B) Relative signal intensities. The values are means from the log base 10 value of flux relative to results for the non-luciferase-expressing control; the error bars represent standard deviations. p/s, photons per second.

the vitreous (30, 38). Negative-stain electron microscopy revealed no gross structural changes in any of the capsid variants (Fig. 2C). Y-F and T-V mutations on the AAV2 capsid have surface proximities of T/V491 and Y/F730 to the HS binding residues (28, 29), while the other residues are distributed throughout the capsid surface. The slight reduction in heparin binding compared to that of WT AAV2 suggests a minor but noticeable effect on the function of the HS residues on the capsid by the Y-F and/or T-V substitution. The specific effect each mutation has on HS affinity requires further investigation. It is worth noting that the AAV2-based variant, AAV7m8, selected for its ability to transduce photoreceptors via the vitreous by Schaffer et al. (like the AAV2 Y-F and T-V variants), also binds heparin but with lower affinity than that of WT AAV2 (48). In the case of AAV7m8, it is presumed that the insertion of the 9mer peptide at position 587/588 leads to steric hindrance of the HS binding residues clustered within this capsid vicinity.

Grafting of HS affinity onto AAV1 confers efficient intravitreal transduction. To probe the effect of HS binding on retinal transduction when vector is delivered via the vitreous, two closely related AAV serotypes, AAV1 and AAV6, which differ by 6/736 residues, including E531K, an HS binding determinant for AAV6 (34), were compared (Fig. 3). AAV6 previously has been reported to efficiently transduce inner retina via the vitreous, while AAV1 promotes only limited transduction when delivered via this route (32). In this study, Ivt delivery of rAAV1, an rAAV1(E531K) mutant (grafted with the AAV6 HS determinant), and rAAV6 vectors expressing mCherry into C57BL/6J mice showed similar retina tropism between rAAV1(E531K) and rAAV6, with transduction observed predominantly in Müller glia (Fig. 3B). The subretinal delivery of all three vectors resulted in the robust transduction of the outer retina (Fig. 3B). It was previously reported that shH10, an AAV6-based variant mined from an AAV library by screening in human astrocytes in culture, efficiently transduces Müller glia following Ivt injection (49). The conclusion made by authors after analyzing the relative transduction of capsid variants containing individual residues and combinations of residues differing between AAV6 and ShH10 was that improvements in the latter resulted from an increase in HS affinity of ShH10 relative to AAV6 (49). Thus, the AAV1(E531K) phenotype likely is due to a gain of HS binding ability.

Effects of grafting HS affinity on photoreceptor-philic serotypes. We next asked whether the grafting of HS binding onto AAV serotypes that display strong photoreceptor transduction via subretinal delivery would result in transduction from Ivt delivery. AAV5- and AAV8-based vectors mediate the robust transduction of photoreceptors by subretinal injection but do not effectively transduce retina when injected intravitreally (30, 50). Previously, it was shown that the substitution of key canonical HS binding residues of AAV2 into AAV5 and AAV8 capsids conferred binding to HS (29, 51). We replaced the structurally equivalent residues in AAV5 and AAV8(Y733F) with amino acids 585 to 588 of AAV2 (RGNR) (Fig. 4A) and confirmed their ability to bind heparin by column chromatography (Fig. 4B). We also determined that there were no gross structural abnormalities of the capsid by negative-stain electron microscopy (Fig. 4C). The evaluation of the transduction efficiencies of WT rAAV5, rAAV5+HS, rAAV8(Y733F), and rAAV8(Y733F)+HS *in vivo* showed no retina transduction for the WT and HS variants when delivered intravitreally (Fig. 5). While the AAV5 and AAV8(Y733F) data were expected, the observations for the HS variants were contradictory to the prediction that HS binding would facilitate retinal transduction from the vitreous. Subretinally delivered AAV8(Y733F) and AAV8(Y733F)+HS transduced both photoreceptors and RPE equally, whereas AAV5+HS transduction by subretinal injection was reduced relative to that of AAV5 (Fig. 5). We note that previous attempts at grafting HS binding onto AAV5 have resulted in virus deemed to be noninfectious (29). In this study, we limited the number of substitutions to the core RGNR residues, where Opie et al. replaced RGNRQA (Fig. 4A) (29). While we did observe clear evidence of transduction mediated by subretinal delivery of the rAAV5+HS vector, the levels were far below that observed for the unmodified rAAV5 (Fig. 5). To confirm that rAAV5+HS was indeed infectious, we infected 661W cells, a cone photoreceptor cell line previously shown to be permissive to AAV5 (39), with rAAV5+HS and rAAV5 carrying mCherry and quantified transduction via FACS. Our results confirmed that the rAAV5+HS vector was infectious; however, transduction efficiency was reduced relative to that of WT AAV5 (Fig. 5B).

HS affinities of AAV2-based vectors with mutations to canonical HS residues. In previous studies, it was shown that

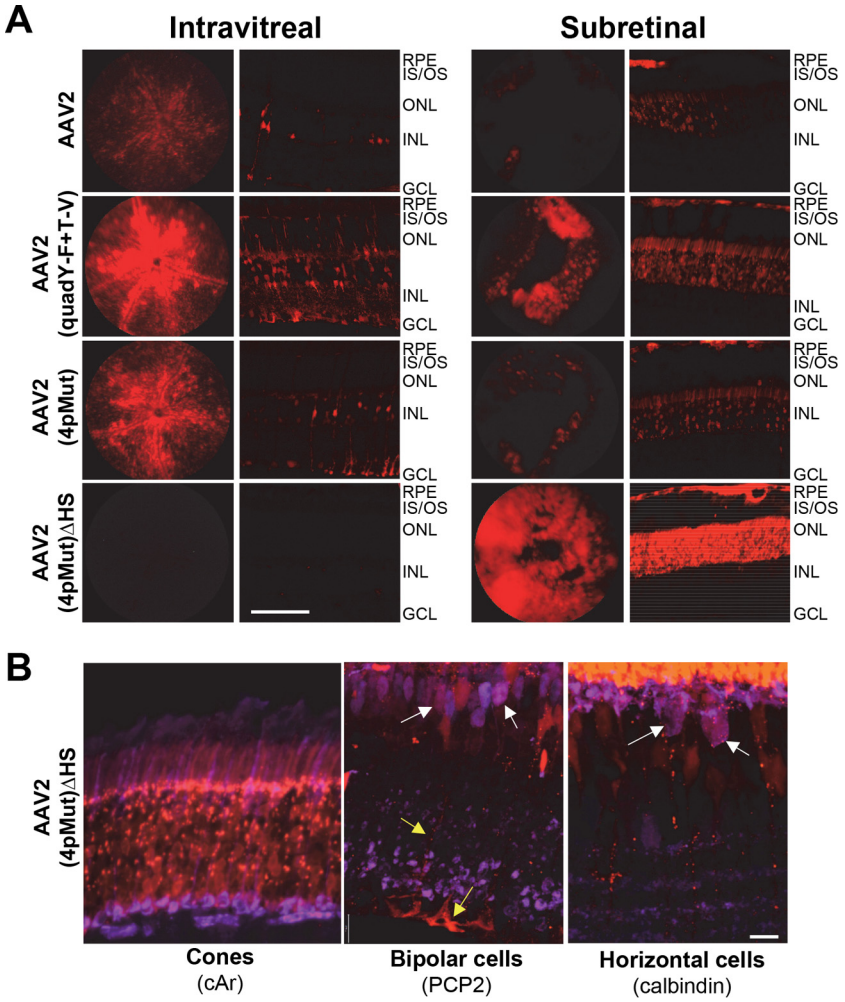

FIG 9 Transduction profiles of rAAV2-based vectors with various HS affinities following subretinal or intravitreal injection in Nrl-GFP mice. rAAV2, rAAV2(quadY-F+T-V), rAAV2(4pMut), and rAAV2(4pMut)ΔHS vectors were delivered at a dose of 5×10^9 vector genomes. Both in-life fundus images and representative retinal sections are shown. IS/OS, inner segments/outer segments of photoreceptors; ONL, outer nuclear layer; INL, inner nuclear layer; GCL, ganglion cell layer. Scale bar in panel A, 50 μm. (B) AAV2(4pMut)ΔHS-mediated mCherry expression in non-rod neural retinal cells. Costaining with antibodies against cone arrestin (left), purkinje cell protein (PCP2) (middle), or calbindin (right) reveal the transduction of cone photoreceptors and, to a much lesser extent, bipolar cells (white arrows), horizontal cells (white arrows), and Muller cells (yellow arrows in the middle panel). IS/OS, inner/outer segments; ONL, outer nuclear layer; INL, inner nuclear layer; GC, ganglion cell layer. Scale bar in panel B, 12 μm.

rAAV2(quadY-F) and rAAV2(quadY-F+T-V) vectors promoted significant transduction of photoreceptors from Ivt injection in both small- and large-animal models (30, 38, 52). Of the AAV2-based variants to be tested, rAAV2(tripleY-F+T-V) has the strongest liver transduction following intravascular delivery and exhibits maximal nuclear translocation (35). We rationalized that a variant with maximal proteasome avoidance and similar HS affinity relative to that of AAV2 would make a good template for mutagenesis. For the sake of simplicity, we refer to AAV2(tripleY-F+T-V) as AAV2(4pMut), in reference to the four proteosome avoidance mutations on the capsid. We confirmed that AAV2(4pMut) bound heparin with affinity similar to that of WT AAV2 (Fig. 6). We then sought to modulate the HS binding of AAV2(4pMut) via selective mutagenesis of AAV2 canonical HS binding residues by replacement with structurally equivalent residues from non-HS binder AAV5 (Table 2) with the goal of further characterizing the effect of HS binding on retina transduction from Ivt delivery. Three substitutions were made in AAV2(4pMut), R487G (R-G), R585S (R-S), and R588T (R-T), yielding a total of 4 variants, AAV2(4pMut)+R-S, AAV2(4pMut)+R-T, AAV2(4pMut)+R-S+R-T, and AAV2(4pMut)+R-S+R-T+R-G [which we refer to as AAV2(4pMut)ΔHS] (Table 2). Collectively, we refer to this group of vectors as the HS variants. The capsid integrity of AAV2(4pMut) and the HS variants was confirmed by EM, and heparin binding was evaluated by column chromatography (Fig. 7A and D). None of the HS variants tested bound heparin to any significant extent. They all produced intact particles (Fig. 7D).

Intact HS residues are required for retinal transduction by AAV2-based vectors via the vitreous. The goal of this set of experiments was to determine if Ivt delivery of the HS variants facilitated transduction. To this end, HS variant vectors were injected at the highest available titer, except for rAAV2(4pMut), which was diluted and delivered at 1×10^{10} vg/μl. The evaluation of transduction by intravitreally delivered rAAV2(4pMut) and the

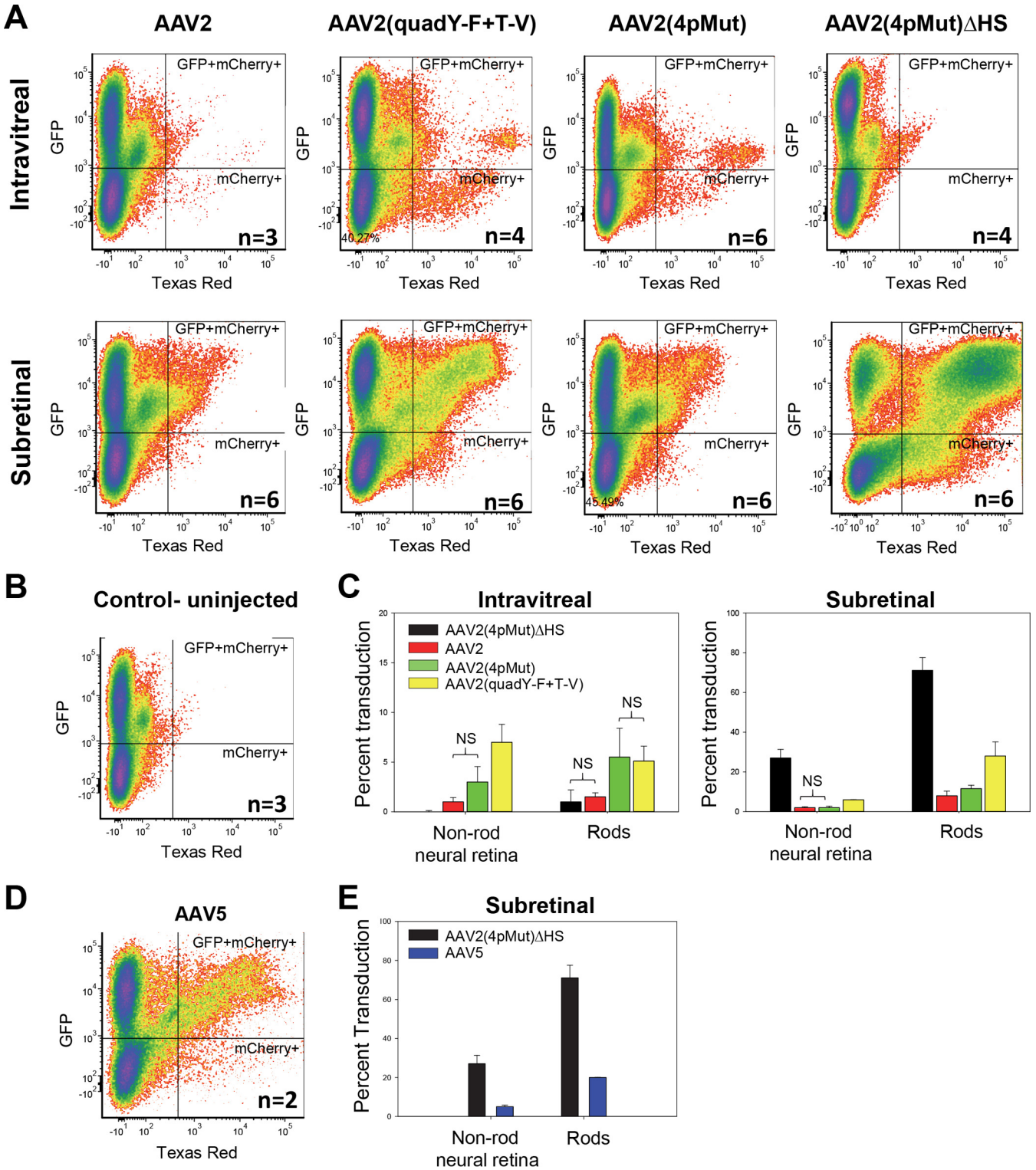

FIG 10 Relative transduction efficiencies of unmodified rAAV2, rAAV2(quadY-F+T-V), rAAV2(4pMut), rAAV2(4pMut)ΔHS, and rAAV5 in rod photoreceptors and non-rod neural retina and glia following intravitreal or subretinal injection in Nrl-GFP mice. (A, B, and D) FACS analysis was used to quantify the percentage of cells that were GFP positive (rods), mCherry positive (neural retinal cells/glia transduced by rAAV), and both GFP and mCherry positive (rods transduced by rAAV). Plots from pooled treated and untreated retinas are shown in panels A, B, and D. (C) Quantification of the percent transduction by rAAV2-based vectors, as determined by mCherry expression, of non-rod neural retina and rods in intravitreally (left) and subretinally (right) injected Nrl-GFP mice. Differences between cohorts were significant in all cases except those labeled NS (not significant). (D) Quantification of the percent transduction by rAAV5, as determined by mCherry expression, of non-rod neural retina and rods in subretinally injected Nrl-GFP mice. Error bars represent ± one standard deviation.

TABLE 4 Comparison of transduction of non-rod neural retinal cells and rod photoreceptors across rAAVs

Cell type and route of infection	Transduction level[a]			
	AAV2(4pMut)ΔHS	AAV2	AAV2(4pMut)	AAV2(quadY-F+T-V)
Ivt				
Non-rod neural retina				
Control uninjected	NS	**	**	**
AAV2(4pMut)ΔHS	—	**	**	**
AAV2		—	NS	**
AAV2(4pMut)			—	*
AAV2(quadY-F+T-V)				—
Rods				
Control uninjected	NS	**	**	**
AAV2(4pMut)ΔHS	—	NS	*	**
AAV2		—	*	*
AAV2(4pMut)			—	NS
AAV2(quadY-F+T-V)				—
Subretinal				
Non-rod neural retina				
Control uninjected	****	****	***	****
AAV2(4pMut)ΔHS	—	****	****	****
AAV2		—	NS	****
AAV2(4pMut)			—	****
AAV2(quadY-F+T-V)				—
Rods				
Control uninjected	****	***	****	***
AAV2(4pMut)ΔHS	—	****	****	****
AAV2		—	NS	****
AAV2(4pMut)			—	**
AAV2(quadY-F+T-V)				—

[a] Statistical comparison of the percent transduction of non-rod neural retinal cells and rod photoreceptors was performed across rAAVs. *, **, ***, and **** indicate statistical significance at P values of <0.05, 0.01, 0.001, and 0.0001, respectively, according to the two-tailed unpaired t test. NS, not significant. —, not applicable.

HS variants revealed that AAV2(4pMut) strongly transduced inner retina following Ivt injection. The observed tropism of AAV2(4pMut) was consistent with the pattern of transduction previously reported for AAV2(tripleY-F) (38). Mutations to any or all of the canonical HS residues resulted in the failure of the HS variants to transduce retina by Ivt injection (Fig. 7B). The HS variants also failed to transduce HEK293 cells *in vitro* (Fig. 7C). However, subretinal injection of all HS capsid variants resulted in clear and robust retinal transduction (Fig. 7B).

Intravascular delivery of AAV2(4pMut)ΔHS does not result in liver transduction. Given the robust transduction of photoreceptors by AAV2(4pMut)ΔHS and the fact that the parent capsid with intact HS binding, AAV2(4pMut), has been shown to be the most efficient AAV2-based capsid for transducing liver (35), we sought to verify that AAV2(4pMut)ΔHS, like other AAV2 capsids deficient in HS binding (53), was detargeted from liver. We compared transduction after intravascular delivery through the retro-orbital venous sinus of AAV2(4pMut)ΔHS relative to AAV2. In addition, we tested the AAV2(quadY-F+T-V) variant, as it has not previously been evaluated via this delivery route. Delivery of 2×10^{11} vg of rAAV2(4pMut)ΔHS did not result in appreciable expression (Fig. 8). In contrast, the typical pattern of liver-restricted expression was observed for AAV2. Despite containing the same 4 mutations (Y444F, Y500, Y730F, and T491V) in AAV2(4pMut) that confer greatly improved liver transduction when multiplexed (35), AAV2(quadY-F+T-V) transduced liver only modestly better than AAV2 (Fig. 8). This is in agreement with the reduced HS affinity of AAV2(quadY-F+T-V) relative to that of AAV2 and HS binding being the main determinant of liver transduction (53). Empty AAV2 capsid with mutations to disrupt HS binding (AAV585/588) has been used as a decoy to adsorb neutralizing antibodies to AAV capsid (54). Additionally, AAV2 Y-F vectors have been shown to reduce T-cell-mediated hepatotoxicity by minimizing cross-presentation through avoidance of the proteasome (55). Significantly, AAV2(4pMut)ΔHS possesses mutations from both classes of variants and thus seems well suited for use as a capsid decoy, because what small fraction of capsid that could achieve cellular entry presumably would be less likely to be processed for cross-presentation.

HS affinity impacts photoreceptor transduction efficiency. Building on the qualitative assessment of transduction by rAAVs described above, we selected a group of AAV2-based variants with which to quantify rod photoreceptor and non-rod transduction following Ivt or subretinal injection. This was accomplished using Nrl-GFP mice, a model with constitutively GFP-expressing and, thus, sortable rod photoreceptors (56). Because rods comprise ~95 to 97% of all photoreceptors in mouse (cones are 3 to 5%), this population of GFP^+ cells nicely represents outer neural retina. Prior to dissociation, the easily visible pigmented RPE is carefully removed from the retina. Therefore, contained within the GFP-negative population are cones, middle/inner retinal neurons (bipolar cells, horizontal cells, astrocytes, amacrine cells, and retinal ganglion cells), and Müller glia. Nrl-GFP mice were injected with equal amounts (5×10^9 vg) of rAAV2, rAAV2(quadY-F+T-V),

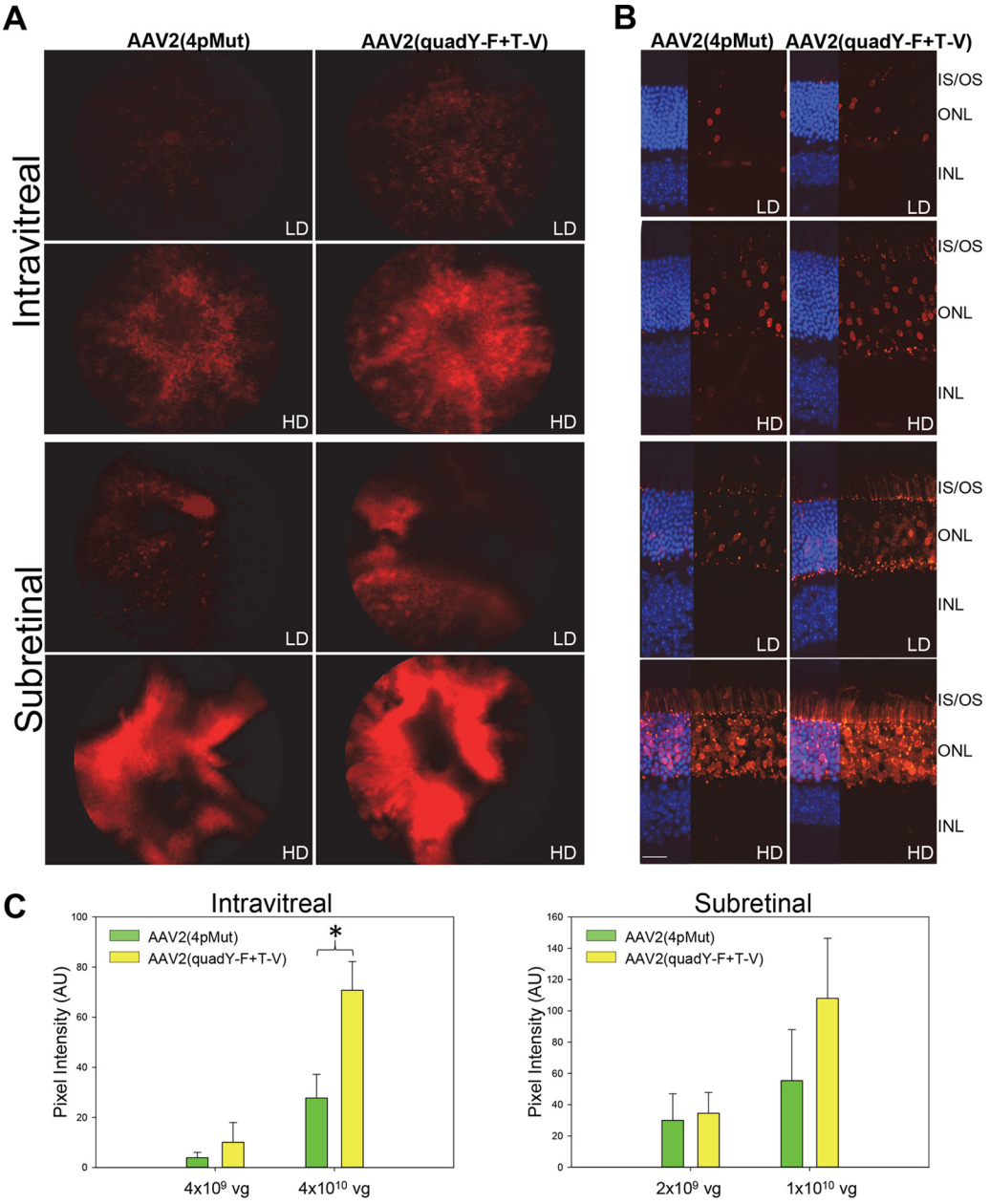

FIG 11 Transduction of rAAV2(4pMut) and rAAV2(quadY-F+T-V) vectors containing a photoreceptor-specific hGRK1 promoter and mCherry transgene following either subretinal or intravitreal injection at two doses in C57BL/6J mice. mCherry expression in representative fundus images (A) and retinal sections (B) reveals relatively higher transduction of photoreceptors (PRs) by AAV2(quadY-F+T-V) following either subretinal or intravitreal injection at both doses. (C) Transduction was quantified using relative mCherry-mediated pixel intensity in fundus images such as those seen in panel A (three per cohort). LD, low dose; HD, high dose; IS/OS, inner/outer segments; ONL, outer nuclear layer; INL, inner nuclear layer; AU, arbitrary units. Scale bar in panel B, 20 μm.

rAAV2(4pMut), or rAAV2(4pMut)ΔHS carrying the mCherry transgene. As expected, fundoscopy and immunohistochemistry of retinal cross sections at 6 weeks postinjection revealed strong transduction by AAV2(quadY-F+T-V) and AAV2(4pMut) following either Ivt or subretinal delivery (Fig. 9A). AAV2 weakly transduced retina via both routes. While AAV2(4pMut)ΔHS failed to transduce retina by Ivt injection (Fig. 9A and B), it strongly transduced outer retina following subretinal delivery and exhibited greater lateral spread than all other vectors tested, as evidenced by the wider relative area of mCherry fluorescence in fundus images (Fig. 9A). This is unlike AAV2, AAV2(quadY-F+T-V), and AAV2(4pMut), which exhibited maximal transduction that was restricted to the area of maximal vector exposure (i.e., within the core of the bleb/retinal detachment) (Fig. 9A). IHC confirmed the strong transduction of cone photoreceptors by AAV2(4pMut)ΔHS. The transduction of Müller glia, bipolar cells, and horizontal cells, while observed, was less common (Fig. 9B).

FACS analysis of dissociated Nrl-GFP retinas was used to quantify the percentage of cells that were GFP^+ (rods), $mCherry^+$ (non-rod retinal neurons and Müller glia transduced by rAAVs),

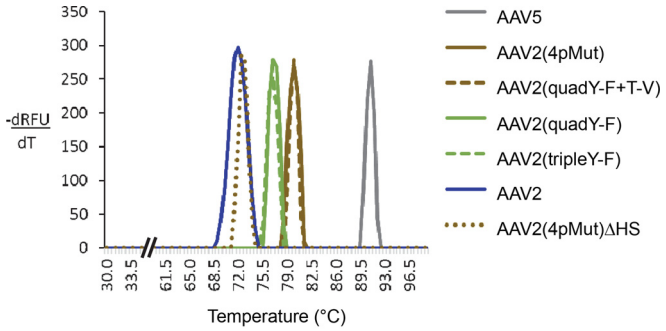

Sample	Tm (°C)	Published Tm (°C)
AAV5	90.8 ±0.3	90.5+0.3
AAV2(4pMut)	79.7 ±0.6	-
AAV2(quadY-F+T-V)	79.5 ±0.9	-
AAV2(quadY-F)	76.0 ±1.3	-
AAV2(tripleY-F)	76.2 ±0.8	-
AAV2	71.8 ±0.3	71.6+0.3
AAV2(4pMut)ΔHS	72.2±0.3	-

FIG 12 Thermal profile of wtAAV2, AAV2-based capsid mutants, and AAV5 vectors which were determined by DSF. The peak temperature or melting temperature of each vector is recorded in the table and the standard deviation calculated from the experiments, all of which were done in triplicates.

or both GFP$^+$ and mCherry$^+$ (rods transduced by rAAVs) (Fig. 10). While the amount of rods transduced by Ivt-delivered AAV2(quadY-F+T-V) or AAV2(4pMut) did not significantly differ, the former transduced significantly more non-rod retinal neurons/glia following Ivt delivery than all other vectors tested ($P = <0.05$) (Fig. 10C and Table 4). Significantly higher retinal transduction was achieved with subretinally delivered AAV2(4pMut)ΔHS than with all other vectors tested ($P = <0.0001$) (Fig. 10C and Table 4). FACS confirmed that AAV2(4pMut)ΔHS transduced ~75% of rods, which represents ~6- and ~2.5-fold increases over AAV2(4pMut) and AAV2(quadY-F+T-V), respectively. It is worth noting that subretinal injection blebs of 1 μl in an adult mouse retina cover approximately 60% to 80% of the retina. Therefore, AAV2(4pMut)ΔHS transduced all rods within the bleb, and likely those outside the bleb as well. Notably, using this method, we found photoreceptor transduction by subretinally delivered AAV2(4pMut)ΔHS to be more robust than that achieved by AAV5, a known photoreceptor-philic serotype (Fig. 10D and E). Subretinal AAV2(quadY-F+T-V) transduced significantly more photoreceptors than AAV2(4pMut) ($P = <0.0001$). Taken together, these results indicate that HS affinity is a key determinant of photoreceptor transduction efficiency for subretinally delivered rAAVs. The lack of HS binding of the other photoreceptor-philic serotypes, AAV5 and AAV8, is consistent with this. Because the vast majority of inherited retinal diseases are caused by photoreceptor-specific defects, interest in identifying the most efficient AAV vectors with which to target these cells remains high. The ideal vector will affect therapy with the fewest number of capsid particles. The high efficiency and enhanced biodistribution for photoreceptors by AAV2(4pMut)ΔHS suggests it is a promising candidate for use in photoreceptor-targeted gene therapies. The ability to transduce areas outside the retinal detachment is advantageous, particularly if it enables the transduction of the macula and fovea without detachment of the structures.

Comparison of photoreceptor-specific transduction by AAV2(quadY-F+T-V) and AAV2(4pMut) following Ivt delivery. Data described above revealed that both AAV2(quadY-F+T-V) and AAV2(4pMut) transduce rod photoreceptors following Ivt injection. We next quantified the relative performance of these variants by utilizing a construct containing the photoreceptor-specific human rhodopsin kinase (hGRK1) promoter driving mCherry in C57Bl/6J mice (14, 57). Mice were injected intravitreally with 4×10^{10} vg (high dose) or 4×10^{9} vg (low dose) or subretinally with 1×10^{10} vg (high dose) or 2×10^{9} vg (low dose). Although C57Bl/6J mice do not have sortable photoreceptors and, thus, FACS cannot be used as described above, hGRK1 has been shown to restrict transgene expression to rods and cones following subretinal injection (14, 57). Representative fundus images and retinal cross sections revealed a clear dose response for each vector following either injection route (Fig. 11A and B). Retinal cross sections confirmed that mCherry expression was limited to photoreceptors for both vector doses and injection routes. Representative images revealed that AAV2(quadY-F+T-V) transduced more photoreceptors than dose-matched AAV2(4pMut). The photoreceptor-restricted expression of mCherry allowed for the quantification of fluorescence intensities in fundus images and thereby a comparison of relative transduction efficiencies (Fig. 11C). Significantly higher transduction was observed for AAV2(quadY-F+T-V) than for AAV2(4pMut) following Ivt injection at the high dose ($P = <0.01$) (Fig. 11C).

AAV2 variants show altered capsid stability with respect to the WT. The capsid stability of AAV2 Y-F/T-V and HS variants, as evaluated by DSF, showed a difference from WT AAV2. All of the Y-F/T-V capsid variants were more stable than WT AAV2, with the T-V change increasing stability by ~3°C more than the Y-F variants (Fig. 12). Of note, the two variants observed to transduce photoreceptors by Ivt injection, AAV2(4pMut) and AAV2 (quadY-F+T-V) (Fig. 12), clustered together in regard to their stability. Further investigation is required to definitively determine whether capsid stability contributes to increased retinal transduction via the vitreous for these vectors. Interestingly, while AAV2(4pMut) was found to be more stable than WT AAV2, the removal of HS residues from AAV2(4pMut) reverted stability to the WT AAV2 level.

Conclusions. In this study, we established that HS binding is a determinant of retinal transduction for AAV1/6 and AAV2. For AAV2-based vectors, the observation that the mutation of established HS binding residues (R487, R585, and R588) produced vectors completely incapable of transducing retina by Ivt injection or HEK293 cells *in vitro* supports the current understanding that AAV2 is dependent on HS as a primary receptor for infection (24). However, the observation of efficient photoreceptor/RPE transduction following subretinal injection of all HS binding-deficient vectors, most notably AAV2(4pMut)ΔHS, provides strong evidence that another receptor, not HS, is mediating infection in these cells. Further characterization of AAV2(4pMut)ΔHS by glycan array analysis, for example, will be required to determine if a gain in receptor utilization has been acquired. In the context of strategies for further enhancing AAV for retinal transduction via the vitreous, it is clear that the maintenance of HS binding is important. The fact that no retinal transduction was observed following intravitreal injection of AAV2(4pMut)ΔHS, and that AAV1(E531K), but not AAV1, is able to transduce the retina via this route suggests that HS binding is required in the early stages of

the process, where capsid first must associate with the vitreoretinal junction. The observation that AAV5+HS and AAV8(733F)+HS bind heparin but fail to promote retinal transduction via the vitreous indicate that the ability to bind HS is not the only requirement for Ivt-mediated transduction. Alternatively, the overly strong affinity to heparin by AAV5+HS and AAV8(Y733F)+HS vectors may prevent them from moving beyond the ILM. Taken together, it is reasonable to suggest that the first step of retinal transduction by intravitreally injected AAV2-based vectors involves HS binding which promotes cellular entry upon contact with the ILM, regardless of the ultimate cell type to be transduced. Furthermore, to improve the photoreceptor transduction efficacy of these vectors, a balancing act likely is required to reduce HS affinity (thereby increasing photoreceptor tropism) in a way that does not interfere with the ability of the capsid to utilize HS for cellular entry at the ILM. Lastly, the observation of increased stability for the capsids that mediate photoreceptor transduction by Ivt injection suggests that this is an area for future exploration.

ACKNOWLEDGMENTS

This work was supported by Foundation Fighting Blindness grants R01EY024280 and P30EY021721 (Vision Research Core grant) and an unrestricted grant from Research to Prevent Blindness.

We thank Sergei Zolotukhin, Arun Srivastava, and George Aslanidi for generously providing Rep-Cap plasmids. We thank the Retinal Gene Therapy Vector Laboratory for the packaging of rAAV vectors. We thank the UF Interdisciplinary Center for Biotechnology Research Electron Microscopy Core for electron microscopy access (funded by the UF College of Medicine and UF Division of Sponsored Programs).

FUNDING INFORMATION

Research to Prevent Blindness (RPB) provided funding to Shannon E. Boye. HHS | NIH | National Eye Institute (NEI) provided funding to Shannon E. Boye, Mavis Agbandje-McKenna, Sanford L. Boye, and Shreyasi Choudhury under grant number R01EY024280. HHS | NIH | National Eye Institute (NEI) provided funding to Shannon E. Boye, Sanford L. Boye, Miranda L. Scalabrino, K. Tyler McCullough, Shreyasi Choudhury, Qing Ruan, and James Peterson under grant number P30EY021721. Foundation Fighting Blindness (FFB) provided funding to Shannon E. Boye and Sanford L. Boye.

REFERENCES

1. **Daya S, Berns KI.** 2008. Gene therapy using adeno-associated virus vectors. Clin Microbiol Rev **21:**583–593. http://dx.doi.org/10.1128/CMR.00008-08.
2. **DiMattia MA, Nam HJ, Van Vliet K, Mitchell M, Bennett A, Gurda BL, McKenna R, Olson NH, Sinkovits RS, Potter M, Byrne BJ, Aslanidi G, Zolotukhin S, Muzyczka N, Baker TS, Agbandje-McKenna M.** 2012. Structural insight into the unique properties of adeno-associated virus serotype 9. J Virol **86:**6947–6958. http://dx.doi.org/10.1128/JVI.07232-11.
3. **Govindasamy L, Padron E, McKenna R, Muzyczka N, Kaludov N, Chiorini JA, Agbandje-McKenna M.** 2006. Structurally mapping the diverse phenotype of adeno-associated virus serotype 4. J Virol **80:**11556–11570. http://dx.doi.org/10.1128/JVI.01536-06.
4. **Govindasamy L, DiMattia MA, Gurda BL, Halder S, McKenna R, Chiorini JA, Muzyczka N, Zolotukhin S, Agbandje-McKenna M.** 2013. Structural insights into adeno-associated virus serotype 5. J Virol **87:**11187–11199. http://dx.doi.org/10.1128/JVI.00867-13.
5. **Lerch TF, Xie Q, Chapman MS.** 2010. The structure of adeno-associated virus serotype 3B (AAV-3B): insights into receptor binding and immune evasion. Virology **403:**26–36. http://dx.doi.org/10.1016/j.virol.2010.03.027.
6. **Mikals K, Nam HJ, Van Vliet K, Vandenberghe LH, Mays LE, McKenna R, Wilson JM, Agbandje-McKenna M.** 2014. The structure of AAVrh32.33, a novel gene delivery vector. J Struct Biol **186:**308–317. http://dx.doi.org/10.1016/j.jsb.2014.03.020.
7. **Nam HJ, Lane MD, Padron E, Gurda B, McKenna R, Kohlbrenner E, Aslanidi G, Byrne B, Muzyczka N, Zolotukhin S, Agbandje-McKenna M.** 2007. Structure of adeno-associated virus serotype 8, a gene therapy vector. J Virol **81:**12260–12271. http://dx.doi.org/10.1128/JVI.01304-07.
8. **Ng R, Govindasamy L, Gurda BL, McKenna R, Kozyreva OG, Samulski RJ, Parent KN, Baker TS, Agbandje-McKenna M.** 2010. Structural characterization of the dual glycan binding adeno-associated virus serotype 6. J Virol **84:**12945–12957. http://dx.doi.org/10.1128/JVI.01235-10.
9. **Xie Q, Lerch TF, Meyer NL, Chapman MS.** 2011. Structure-function analysis of receptor-binding in adeno-associated virus serotype 6 (AAV-6). Virology **420:**10–19. http://dx.doi.org/10.1016/j.virol.2011.08.011.
10. **Boye SE, Boye SL, Lewin AS, Hauswirth WW.** 2013. A comprehensive review of retinal gene therapy. Mol Ther **21:**509–519. http://dx.doi.org/10.1038/mt.2012.280.
11. **Bainbridge JW, Smith AJ, Barker SS, Robbie S, Henderson R, Balaggan K, Viswanathan A, Holder GE, Stockman A, Tyler N, Petersen-Jones S, Bhattacharya SS, Thrasher AJ, Fitzke FW, Carter BJ, Rubin GS, Moore AT, Ali RR.** 2008. Effect of gene therapy on visual function in Leber's congenital amaurosis. N Engl J Med **358:**2231–2239. http://dx.doi.org/10.1056/NEJMoa0802268.
12. **Cideciyan AV, Aleman TS, Boye SL, Schwartz SB, Kaushal S, Roman AJ, Pang JJ, Sumaroka A, Windsor EA, Wilson JM, Flotte TR, Fishman GA, Heon E, Stone EM, Byrne BJ, Jacobson SG, Hauswirth WW.** 2008. Human gene therapy for RPE65 isomerase deficiency activates the retinoid cycle of vision but with slow rod kinetics. Proc Natl Acad Sci USA **105:**15112–15117. http://dx.doi.org/10.1073/pnas.0807027105.
13. **Maguire AM, Simonelli F, Pierce EA, Pugh EN, Jr, Mingozzi F, Bennicelli J, Banfi S, Marshall KA, Testa F, Surace EM, Rossi S, Lyubarsky A, Arruda VR, Konkle B, Stone E, Sun J, Jacobs J, Dell'Osso L, Hertle R, Ma JX, Redmond TM, Zhu X, Hauck B, Zelenaia O, Shindler KS, Maguire MG, Wright JF, Volpe NJ, McDonnell JW, Auricchio A, High KA, Bennett J.** 2008. Safety and efficacy of gene transfer for Leber's congenital amaurosis. N Engl J Med **358:**2240–2248. http://dx.doi.org/10.1056/NEJMoa0802315.
14. **Boye SE, Alexander JJ, Boye SL, Witherspoon CD, Sandefer KJ, Conlon TJ, Erger K, Sun J, Ryals R, Chiodo VA, Clark ME, Girkin CA, Hauswirth WW, Gamlin PD.** 2012. The human rhodopsin kinase promoter in an AAV5 vector confers rod- and cone-specific expression in the primate retina. Hum Gene Ther **23:**1101–1115. http://dx.doi.org/10.1089/hum.2012.125.
15. **Mancuso K, Hauswirth WW, Li Q, Connor TB, Kuchenbecker JA, Mauck MC, Neitz J, Neitz M.** 2009. Gene therapy for red-green colour blindness in adult primates. Nature **461:**784–787. http://dx.doi.org/10.1038/nature08401.
16. **Lotery AJ, Yang GS, Mullins RF, Russell SR, Schmidt M, Stone EM, Lindbloom JD, Chiorini JA, Kotin RM, Davidson BL.** 2003. Adeno-associated virus type 5: transduction efficiency and cell-type specificity in the primate retina. Hum Gene Ther **14:**1663–1671. http://dx.doi.org/10.1089/104303403322542301.
17. **Mancuso K, Hendrickson AE, Connor TB, Jr, Mauck MC, Kinsella JJ, Hauswirth WW, Neitz J, Neitz M.** 2007. Recombinant adeno-associated virus targets passenger gene expression to cones in primate retina. J Opt Soc Am A Opt Image Sci Vis **24:**1411–1416. http://dx.doi.org/10.1364/JOSAA.24.001411.
18. **Vandenberghe LH, Bell P, Maguire AM, Cearley CN, Xiao R, Calcedo R, Wang L, Castle MJ, Maguire AC, Grant R, Wolfe JH, Wilson JM, Bennett J.** 2011. Dosage thresholds for AAV2 and AAV8 photoreceptor gene therapy in monkey. Sci Transl Med **3:**88ra54.
19. **Vandenberghe LH, Bell P, Maguire AM, Xiao R, Hopkins TB, Grant R, Bennett J, Wilson JM.** 2013. AAV9 targets cone photoreceptors in the nonhuman primate retina. PLoS One **8:**e53463. http://dx.doi.org/10.1371/journal.pone.0053463.
20. **Jacobson SG, Cideciyan AV, Ratnakaram R, Heon E, Schwartz SB, Roman AJ, Peden MC, Aleman TS, Boye SL, Sumaroka A, Conlon TJ, Calcedo R, Pang JJ, Erger KE, Olivares MB, Mullins CL, Swider M, Kaushal S, Feuer WJ, Iannaccone A, Fishman GA, Stone EM, Byrne BJ, Hauswirth WW.** 2012. Gene therapy for leber congenital amaurosis caused by RPE65 mutations: safety and efficacy in 15 children and adults followed up to 3 years. Arch Ophthalmol **130:**9–24. http://dx.doi.org/10.1001/archophthalmol.2011.298.
21. **Jacobson SG, Acland GM, Aguirre GD, Aleman TS, Schwartz SB,**

Cideciyan AV, Zeiss CJ, Komaromy AM, Kaushal S, Roman AJ, Windsor EA, Sumaroka A, Pearce-Kelling SE, Conlon TJ, Chiodo VA, Boye SL, Flotte TR, Maguire AM, Bennett J, Hauswirth WW. 2006. Safety of recombinant adeno-associated virus type 2-RPE65 vector delivered by ocular subretinal injection. Mol Ther **13:**1074–1084. http://dx.doi.org/10.1016/j.ymthe.2006.03.005.

22. **Royal College of Ophthalmologists.** 2009. Guidelines for intravitreal injections procedure 2009. Royal College of Ophthalmologists, London, United Kingdom.
23. **Dalkara D, Kolstad KD, Caporale N, Visel M, Klimczak RR, Schaffer DV, Flannery JG.** 2009. Inner limiting membrane barriers to AAV-mediated retinal transduction from the vitreous. Mol Ther **17:**2096–2102. http://dx.doi.org/10.1038/mt.2009.181.
24. **Summerford C, Samulski RJ.** 1998. Membrane-associated heparan sulfate proteoglycan is a receptor for adeno-associated virus type 2 virions. J Virol **72:**1438–1445.
25. **Chai L, Morris JE.** 1994. Distribution of heparan sulfate proteoglycans in embryonic chicken neural retina and isolated inner limiting membrane. Curr Eye Res **13:**669–677. http://dx.doi.org/10.3109/02713689408999903.
26. **O'Donnell J, Taylor KA, Chapman MS.** 2009. Adeno-associated virus-2 and its primary cellular receptor–cryo-EM structure of a heparin complex. Virology **385:**434–443. http://dx.doi.org/10.1016/j.virol.2008.11.037.
27. **Levy HC, Bowman VD, Govindasamy L, McKenna R, Nash K, Warrington K, Chen W, Muzyczka N, Yan X, Baker TS, Agbandje-McKenna M.** 2009. Heparin binding induces conformational changes in adeno-associated virus serotype 2. J Struct Biol **165:**146–156. http://dx.doi.org/10.1016/j.jsb.2008.12.002.
28. **Kern A, Schmidt K, Leder C, Muller OJ, Wobus CE, Bettinger K, Von der Lieth CW, King JA, Kleinschmidt JA.** 2003. Identification of a heparin-binding motif on adeno-associated virus type 2 capsids. J Virol **77:**11072–11081. http://dx.doi.org/10.1128/JVI.77.20.11072-11081.2003.
29. **Opie SR, Warrington KH, Jr, Agbandje-McKenna M, Zolotukhin S, Muzyczka N.** 2003. Identification of amino acid residues in the capsid proteins of adeno-associated virus type 2 that contribute to heparan sulfate proteoglycan binding. J Virol **77:**6995–7006. http://dx.doi.org/10.1128/JVI.77.12.6995-7006.2003.
30. **Kay CN, Ryals RC, Aslanidi GV, Min SH, Ruan Q, Sun J, Dyka FM, Kasuga D, Ayala AE, Van VK, Agbandje-McKenna M, Hauswirth WW, Boye SL, Boye SE.** 2013. Targeting photoreceptors via intravitreal delivery using novel, capsid-mutated AAV vectors. PLoS One **8:**e62097. http://dx.doi.org/10.1371/journal.pone.0062097.
31. **Kong F, Li W, Li X, Zheng Q, Dai X, Zhou X, Boye SL, Hauswirth WW, Qu J, Pang JJ.** 2010. Self-complementary AAV5 vector facilitates quicker transgene expression in photoreceptor and retinal pigment epithelial cells of normal mouse. Exp Eye Res **90:**546–554. http://dx.doi.org/10.1016/j.exer.2010.01.011.
32. **Hellstrom M, Ruitenberg MJ, Pollett MA, Ehlert EM, Twisk J, Verhaagen J, Harvey AR.** 2009. Cellular tropism and transduction properties of seven adeno-associated viral vector serotypes in adult retina after intravitreal injection. Gene Ther **16:**521–532. http://dx.doi.org/10.1038/gt.2008.178.
33. **Lebherz C, Maguire A, Tang W, Bennett J, Wilson JM.** 2008. Novel AAV serotypes for improved ocular gene transfer. J Gene Med **10:**375–382. http://dx.doi.org/10.1002/jgm.1126.
34. **Wu Z, Asokan A, Grieger JC, Govindasamy L, Agbandje-McKenna M, Samulski RJ.** 2006. Single amino acid changes can influence titer, heparin binding, and tissue tropism in different adeno-associated virus serotypes. J Virol **80:**11393–11397. http://dx.doi.org/10.1128/JVI.01288-06.
35. **Aslanidi GV, Rivers AE, Ortiz L, Song L, Ling C, Govindasamy L, Van Vliet K, Tan M, Agbandje-McKenna M, Srivastava A.** 2013. Optimization of the capsid of recombinant adeno-associated virus 2 (AAV2) vectors: the final threshold? PLoS One **8:**e59142. http://dx.doi.org/10.1371/journal.pone.0059142.
36. **Zhong L, Li B, Mah CS, Govindasamy L, Agbandje-McKenna M, Cooper M, Herzog RW, Zolotukhin I, Warrington KH, Jr, Weigel-Van Aken KA, Hobbs JA, Zolotukhin S, Muzyczka N, Srivastava A.** 2008. Next generation of adeno-associated virus 2 vectors: point mutations in tyrosines lead to high-efficiency transduction at lower doses. Proc Natl Acad Sci USA **105:**7827–7832. http://dx.doi.org/10.1073/pnas.0802866105.
37. **Markusic DM, Herzog RW, Aslanidi GV, Hoffman BE, Li B, Li M, Jayandharan GR, Ling C, Zolotukhin I, Ma W, Zolotukhin S, Srivastava A, Zhong L.** 2010. High-efficiency transduction and correction of murine hemophilia B using AAV2 vectors devoid of multiple surface-exposed tyrosines. Mol Ther **18:**2048–2056. http://dx.doi.org/10.1038/mt.2010.172.
38. **Petrs-Silva H, Dinculescu A, Li Q, Deng WT, Pang JJ, Min SH, Chiodo V, Neeley AW, Govindasamy L, Bennett A, Agbandje-McKenna M, Zhong L, Li B, Jayandharan GR, Srivastava A, Lewin AS, Hauswirth WW.** 2011. Novel properties of tyrosine-mutant AAV2 vectors in the mouse retina. Mol Ther **19:**293–301. http://dx.doi.org/10.1038/mt.2010.234.
39. **Ryals RC, Boye SL, Dinculescu A, Hauswirth WW, Boye SE.** 2011. Quantifying transduction efficiencies of unmodified and tyrosine capsid mutant AAV vectors in vitro using two ocular cell lines. Mol Vis **17:**1090–1102.
40. **Zolotukhin S, Potter M, Zolotukhin I, Sakai Y, Loiler S, Fraites TJ, Jr, Chiodo VA, Phillipsberg T, Muzyczka N, Hauswirth WW, Flotte TR, Byrne BJ, Snyder RO.** 2002. Production and purification of serotype 1, 2, and 5 recombinant adeno-associated viral vectors. Methods **28:**158–167. http://dx.doi.org/10.1016/S1046-2023(02)00220-7.
41. **Cresawn KO, Fraites TJ, Wasserfall C, Atkinson M, Lewis M, Porvasnik S, Liu C, Mah C, Byrne BJ.** 2005. Impact of humoral immune response on distribution and efficacy of recombinant adeno-associated virus-derived acid alpha-glucosidase in a model of glycogen storage disease type II. Hum Gene Ther **16:**68–80. http://dx.doi.org/10.1089/hum.2005.16.68.
42. **Emsley P, Cowtan K.** 2004. Coot: model-building tools for molecular graphics. Acta Crystallogr D Biol Crystallogr **60:**2126–2132. http://dx.doi.org/10.1107/S0907444904019158.
43. **Xiao C, Rossmann MG.** 2007. Interpretation of electron density with stereographic roadmap projections. J Struct Biol **158:**182–187. http://dx.doi.org/10.1016/j.jsb.2006.10.013.
44. **DeLano W.** 2002. The PyMOL molecular graphics system. DeLano Scientific LLC, San Carlos, CA.
45. **Timmers AM, Zhang H, Squitieri A, Gonzalez-Pola C.** 2001. Subretinal injections in rodent eyes: effects on electrophysiology and histology of rat retina. Mol Vis **7:**131–137.
46. **Yardeni T, Eckhaus M, Morris HD, Huizing M, Hoogstraten-Miller S.** 2011. Retro-orbital injections in mice. Lab Anim (NY) **40:**155–160. http://dx.doi.org/10.1038/laban0511-155.
47. **Boye SL, Conlon T, Erger K, Ryals R, Neeley A, Cossette T, Pang J, Dyka FM, Hauswirth WW, Boye SE.** 2011. Long-term preservation of cone photoreceptors and restoration of cone function by gene therapy in the guanylate cyclase-1 knockout (GC1KO) mouse. Investig Ophthalmol Vis Sci **52:**7098–7108. http://dx.doi.org/10.1167/iovs.11-7867.
48. **Dalkara D, Byrne LC, Klimczak RR, Visel M, Yin L, Merigan WH, Flannery JG, Schaffer DV.** 2013. In vivo-directed evolution of a new adeno-associated virus for therapeutic outer retinal gene delivery from the vitreous. Sci Transl Med **5:**189ra176.
49. **Klimczak RR, Koerber JT, Dalkara D, Flannery JG, Schaffer DV.** 2009. A novel adeno-associated viral variant for efficient and selective intravitreal transduction of rat Muller cells. PLoS One **4:**e7467. http://dx.doi.org/10.1371/journal.pone.0007467.
50. **Surace EM, Auricchio A.** 2008. Versatility of AAV vectors for retinal gene transfer. Vision Res **48:**353–359. http://dx.doi.org/10.1016/j.visres.2007.07.027.
51. **Vandenberghe LH, Wang L, Somanathan S, Zhi Y, Figueredo J, Calcedo R, Sanmiguel J, Desai RA, Chen CS, Johnston J, Grant RL, Gao G, Wilson JM.** 2006. Heparin binding directs activation of T cells against adeno-associated virus serotype 2 capsid. Nat Med **12:**967–971. http://dx.doi.org/10.1038/nm1445.
52. **Boyd RF, Sledge DG, Boye SL, Boye SE, Hauswirth WW, Komaromy AM, Petersen-Jones SM, Bartoe JT.** 2015. Photoreceptor-targeted gene delivery using intravitreally administered AAV vectors in dogs. Gene Ther http://dx.doi.org/10.1038/gt.2015.96.
53. **Perabo L, Goldnau D, White K, Endell J, Boucas J, Humme S, Work LM, Janicki H, Hallek M, Baker AH, Buning H.** 2006. Heparan sulfate proteoglycan binding properties of adeno-associated virus retargeting mutants and consequences for their in vivo tropism. J Virol **80:**7265–7269. http://dx.doi.org/10.1128/JVI.00076-06.
54. **Mingozzi F, Anguela XM, Pavani G, Chen Y, Davidson RJ, Hui DJ, Yazicioglu M, Elkouby L, Hinderer CJ, Faella A, Howard C, Tai A, Podsakoff GM, Zhou S, Basner-Tschakarjan E, Wright JF, High KA.**

2013. Overcoming preexisting humoral immunity to AAV using capsid decoys. Sci Transl Med **5:**194ra192.

55. **Martino AT, Basner-Tschakarjan E, Markusic DM, Finn JD, Hinderer C, Zhou S, Ostrov DA, Srivastava A, Ertl HC, Terhorst C, High KA, Mingozzi F, Herzog RW.** 2013. Engineered AAV vector minimizes in vivo targeting of transduced hepatocytes by capsid-specific CD8+ T cells. Blood **121:**2224–2233. http://dx.doi.org/10.1182/blood-2012-10-460733.
56. **Akimoto M, Cheng H, Zhu D, Brzezinski JA, Khanna R, Filippova E, Oh EC, Jing Y, Linares JL, Brooks M, Zareparsi S, Mears AJ, Hero A, Glaser T, Swaroop A.** 2006. Targeting of GFP to newborn rods by Nrl promoter and temporal expression profiling of flow-sorted photoreceptors. Proc Natl Acad Sci USA **103:**3890–3895. http://dx.doi.org/10.1073/pnas.0508214103.
57. **Khani SC, Pawlyk BS, Bulgakov OV, Kasperek E, Young JE, Adamian M, Sun X, Smith AJ, Ali RR, Li T.** 2007. AAV-mediated expression targeting of rod and cone photoreceptors with a human rhodopsin kinase promoter. Investig Ophthalmol Vis Sci **48:**3954–3961. http://dx.doi.org/10.1167/iovs.07-0257.